NASA Technical Memorandum 89050

MACH 6 EXPERIMENTAL AND THEORETICAL STABILITY AND PERFORMANCE OF A FINNED CYLINDRICAL BODY AT ANGLES OF ATTACK UP TO 65°

Edward R. Hartman and Patrick J. Johnston

September 1986

NASA
National Aeronautics and Space Administration

Langley Research Center
Hampton, Virginia 23665

ABSTRACT

A theoretical and experimental investigation of the longitudinal and lateral-directional stability and control of a finned cylindrical body has been conducted at Mach 6. The angle-of-attack range extended from 20° to 65° to encompass maximum lift. Stability, performance, and trim could be accurately predicted with the fins in the + arrangement but this was not the case when the fins were in the × orientation where windward fin choking occurred at angles of attack above 50° reducing their effectiveness and causing pitch up.

SUMMARY

Stability, control, and performance characteristics of a finned cylindrical body was determined theoretically and experimentally at Mach 6. The fins, which were deflected up to 20° for both pitch and roll control, were oriented in either the + or × arrangement. The angle-of-attack range extended from 20° to 65° to encompass maximum lift.

Good agreement between theory and experiment was achieved with the fins in the + orientation. Theory consistantly underpredicted experimental values for the × configuration. Fin choking was observed to occur at angles of attack greater than 50° which caused a dramatic reduction in windward fin effectiveness. Negative deflections alleviated the problem and positive fin deflections exacerbated the choking phenomenon to the extent that pitch-up occurred at high angles of attack.

INTRODUCTION

Experimental hypersonic data on cylindrical bodies with fins at very high angles of attack, that is, beyond that required for maximum lift, are limited. Reference 1 contains force data at Mach 6.83 on a family of cone-cylinder bodies, however, this reference does not contain any moment data. References 2 and 3 contain force, moment, and pressure distribution data on axisymmetric bodies at angles of attack up to 60° but the Mach number range only extends up to 4.63.

Recently developed Euler codes for calculating the aerodynamic characteristics of finned cylindrical bodies, reference 4, fail when pockets of subsonic flow are encountered. Based on tangent-cone impact theory concepts, subsonic

flow would occur on the stagnation line when the flow deflection angle exceeds 53° at Mach 6. Even a reasonably slender forebody half angle of 15° would therefore limit the range of applicability of these codes to an angle of attack of less than about 38° which is far below that required to develop maximum lift. As a result of these mathematical and physical constraints, many aerodynamicists resort to Newtonian hypersonic impact methods to predict vehicle high angle-of-attack forces and moments. Impact methods, of course, imply isolated panels and components with no mutual interference whereas the actual flow about a finned cylindrical body at high angles of attack will have strong interference effects between the body and fins. Impact theory provides a benchmark comparison by which to judge the efficacy of future theoretical efforts; this was the primary intent for including it in the present report.

The purpose of the present study was to experimentally determine the high angle-of-attack hypersonic stability and performance of an axisymmetric body with cruciform fins. The configuration had a simple 12°/6° biconic nose. The delta planform fins were oriented in both the "+" and "×" configurations and were deflected to obtain pitch and roll. The test angle-of-attack range extended from 20° to 65° to encompass the angle of attack for maximum lift. The angle of sideslip was varied from 0° to -3° in order to obtain lateral-directional derivatives. The free-stream Mach number was 5.95 and the length Reynolds number was 2.57×10^6. Extensive comparisions were made with results obtained from the Hypersonic Arbitary Body Aerodynamic Program, reference 5, in order to provide some guidance in its use on finned bodies at high angles of attack.

SYMBOLS

C_A axial-force coefficient, $\frac{\text{Axial force}}{qS}$

$C_{A,b}$ base axial-force coefficient, $\frac{\text{Base axial force}}{qS}$

C_D drag coefficient, $\frac{\text{Drag}}{qS}$

C_L lift coefficient, $\frac{\text{Lift}}{qS}$

C_l rolling-moment coefficient, $\frac{\text{Rolling moment}}{qSd}$

C_{l_β} effective dihedral parameter $\frac{\Delta C_l}{\Delta \beta}$, per deg

C_m pitching-moment coefficient, $\frac{\text{Pitching moment}}{qSd}$

C_N normal-force coefficient, $\frac{\text{Normal force}}{qS}$

C_n yawing-moment coefficient, $\frac{\text{Yawing moment}}{qSd}$

C_{n_β} directional stability parameter $\frac{\Delta C_n}{\Delta \beta}$, per deg

C_p pressure coefficient

C_{Y_β} side-force parameter $\frac{\Delta C_Y}{\Delta \beta}$, per deg

C_Y side-force coefficient, $\frac{\text{Side force}}{qS}$

d reference length (maximum body diameter), 1.300 in.

ℓ body length, 10.827 in.

M free-stream Mach number

q free-stream dynamic pressure, psia

S reference area based on body diameter, $1.327 in^2$

X_{cg} center of gravity, moment reference point

α angle of attack, deg

β angle of sideslip, deg

δ_p pitch-control deflection of fins (negative with leading edge down), deg

δ_r roll-control deflection of fins (positive to provide positive rolling moment), deg

Subscripts

lam laminar boundary layer

max maximum

turb turbulent boundary layer

trim at $C_m = 0$

Model Nomenclature

B body

BT body plus fins (+ or ×, as indicated)

\+ fins in the "+" configuration

× fins in the "×" configuration

Abbreviations

HABP Hypersonic Arbitrary Body Aerodynamics Computer Program

The fins were numbered 1, 2, 3, and 4 clockwise from the top fin (+) or top right (×) as viewed looking upstream. Pitch deflections were made by deflecting fins 2 and 4 (+) or all fins (×) . Roll deflections were made by deflecting fin 2 (leading edge down) and fin 4 (leading edge up) for the + configuration and fins 1 and 2 (leading edge down) and fins 3 and 4 (leading edge up) for the × configuration. All deflection angles are defined as that value each individual fin was deflected.

MODEL, APPARATUS, AND TESTS

A photograph of the model is shown in figure 1 and a sketch is presented in figure 2. The model was constructed of stainless steel and attached to a 6-component water cooled strain gage balance which was sting supported. Base pressures were measured at four locations 90° apart in the "+" orientation and the balance axial forces were adjusted to a condition where free-stream pressure acted over the base. Representative base axial-force coefficients calculated from these pressures are shown in figure 3 where it may be noted that, at high angles of attack, both the presence of the fins and their orientation had a large effect on base axial force.

The model angle of attack was measured on a calibrated scale outside the tunnel by reflecting a point source of light from a prism inbedded in the model surface onto the scale. This method accounted for the deflection of the balance and sting under aerodynamic loads.

The tests were conducted in the Langley 20-Inch Mach 6 tunnel at a nominal stagnation pressure and temperature of 150 psia and 860°R, respectively. At these conditions the average stream Mach number was 5.95.

Fin deflections were set outside the tunnel using a cathetometer and were checked after every test to insure the settings did not change as a result of the combination of aerodynamic heating and air loads. The fins were held in place by a simple set-screw friction arrangement. Deflection angle accuracy was within 0.5°.

THEORETICAL METHODS

The static aerodynamic forces and moments on the configuration were calculated by using the Hypersonic Arbitrary Body Aerodynamics Program (ref. 5). This computer code has numerous options for predicting either windward or leeward pressures as a function of local panel deflection angle. Because of the large deflections involved at high angles of attack, it was believed appropriate to use modified Newtonian theory with $C_{p_{max}} = 1.82$ for Mach 6 on the windward surfaces of the body and fins and a Prandtl-Meyer expansion from the free-stream direction on the leeward surfaces. The justification for using this combination of theories on the body was based primarily on the results shown in reference 1 where the same theory was used on the windward surfaces but stream pressure (C_p = ˆ.00) was assumed to occur on leeward surfaces. It was noted that, without exception, lift coefficients in reference 1 were underpredicted, ostensibly because leeside forces were not accounted for.

With respect to the fin forces, the above combination is probably as good as any because the actual flow is so complex, involving, for example, bow shock intersections with the fins, local flow and gap effects, fin shock detachment and separation.

PRESENTATION OF RESULTS

In order to provide a better understanding of the flow about the configuration, component build-up force and moment data are presented in figure 4 with the control fins undeflected. Incremental forces and moments developed by the undeflected fins are shown in figure 5. These data are supplemented with schlieren photographs in figure 6 to illustrate the complex flow about the fins, especially when they are oriented in the × configuration. Lift, drag, and longitudinal stability with the undeflected fins are shown in figures 7 and 8. Component build-up data in sideslip are shown in figure 9. Force and moment characteristics are shown in figure 10 and schlieren photographs illustrating the effect of control deflection on fin choking are shown in figure 11. Lift, drag, and longitudinal trim characteristics are presented in figures 12 and 13. Center-of-gravity effects on lift coefficients are given in figure 14. Figure 15 presents the effectiveness of the fins at various angles of attack. The effects of control deflections on sideslip derivatives are shown in figure 16. Figure 17 shows roll control effectiveness.

DISCUSSION

Component Build-Up

The longitudinal forces and moments on the body-fin combinations with the undeflected fins are shown in figure 4. Body-alone results are included for reference.

Considering first the body-alone results, it can be seen that the theory predicted the nonlinear normal force with exceptional accuracy over the entire angle-of-attack range. The theoretical pitching moments, however, were more negative than those measured experimentally. This situation suggests that, although the magnitude of the load on the body was correctly predicted, its distribution over the length of the body was not. This difference may be explained by the fact that impact theory does not account for the physics of the local flow, especially the expansion waves emanating from the cone-frustum-cylinder corners which reflect back on the body as compression waves and which presumably would increase the loading forward of the moment reference point and therefore produce a more positive moment than predicted. As a result of axial symmetry, the differences between experiment and theory should vanish at $\alpha \approx 0°$ with the experimental slope $\frac{dC_m}{d\alpha}$ being more positive.

Figure 4(a) shows that the addition of the + fins increased both normal force and pitching moment and the fin contribution was accurately predicted by theory despite the fact that the vehicle bow shock most likely crossed the horizontal fins subjecting them to increased local dynamic pressures. In addition, there are large boundary-layer cross flows on the fuselage which would separate at the fin root and reduce the panel load. Since none of these effects are accounted for by inviscid impact theory concepts, the theoretical fin contributions shown in figure 4(a) must be regarded as entirely fortuitous.

Both laminar and turbulent skin friction estimates were made and it can be seen by the axial-force comparisons in figure 4(a) that the overall agreement was better using the turbulent theory; hence it will be used in the remaining figures.

Figure 4(b) shows that the addition of the × fins increased normal force and pitching moment but, unlike the + fins, the increments of these fins were substantially underpredicted by modified Newtonian theory. Above an angle of attack of about 50° these fins exhibited a distinct pitch-up tendency not

predicted theoretically. To examine this further, the incremental forces and moments of both the + and × fins are shown in figure 5 along with the theoretical results. The agreement between theory and experiment for the + fins has been aluded to earlier. Of greater concern is the fact that, up to about α = 50°, the × fins have almost twice the effectiveness predicted. This force and moment contribution peaks at α = 60° and diminishes thereafter.

The theoretical curves in figure 5(b) show the contributions of the windward and leeward pair of fins as well as the summation of all four fins. Much of the area of the leeside fins is shielded by the body at angles of attack, consequently, their actual effectiveness would be substantially less than that shown. A previous study (ref. 6) indicated that the effectiveness of leeside fins could be accurately accounted for by simple geometric shielding in which the isolated panel forces are reduced by the ratio of shielded area to planform area. If the contribution of the leeside fins are entirely discounted, then the substantial differences between the theory and experiment for the windward fins must be ascribed either to large upwash angles as the local flow curves outboard around the body or to local q effects in the body flow field. At Mach 6, for either two dimensional or conical compressions, it can be calculated that local dynamic pressures increase to a maximum of about three times freestream values at deflection angles near 25° and subsequently diminish for larger deflection angles. Most likely it is a combination of both upwash and local q effects which account for the differences between theory and experiment shown in figure 5(b).

Schlieren photographs.- To aid in understanding the flow behavior about the configuration, especially with the × fins, schlieren pictures were taken at 10° angle of attack intervals in addition to being continuously recorded on video tape.

Figure 6(a) shows the flow about the isolated body. The vehicle bow shock lies very close to the body thus approaching pure Newtonian flow conditions where the shock is assumed to coincide with the body surface. It is not surprising, then, that Newtonian theory was able to accurately predict normal force. Another feature noticeable in figure 6(a) is the rapid curvature of the bow shock when it encounters the expansion fan at the body base.

Figure 6(b) shows the flow about the + configuration. The bow shock crosses the lower fin at about the midpoint of the exposed semi-span and

essentially remains there over the entire angle-of-attack range; thus, part of the ventral fin is exposed to free-stream dynamic pressure and the remainder experiences a varying local dynamic pressure behind the bow shock. As noted previously, at Mach 6, local q ratios may approach three times free-stream values, consequently local fin loads may be increased by a corresponding amount. Since the schlieren photographs only show a silhouette of the flow in the meridian plane, it could not be determined whether the bow shock crossed the horizontal fins which are the primary stabilizing surfaces.

Figure 6(c) shows the schlieren photographs of the flow about the × configuration. At α = 35°, the bow shock in the vertical plane of symmetry is near the projection of the fin tip-chord plane. Thus it probably intersected the windward fins since they are rolled out 45° from the meridian plane. It is also evident at this angle of attack that the lower fin leading-edge shock is detached from the leading edge. For reference, a 70° swept flat plate will have a detached bow shock below Mach 2.92 which suggests that the local Mach number ahead of the fins was somewhat below this value.

As the angle of attack increases to 45°, the detached fin leading-edge shock appears to intersect the main bow shock in the vicinity of the fin tip chord and the dark streak downstream of the fin suggests either a strong tip vortex (denoting a large panel loading) or a slip line originating at the intersection of the two shocks.

At an angle of attack of 55°, significant changes in the flow pattern about the windward fins are evident and, as noted previously in figure 5(b), the rate of change in fin contribution to normal force abruptly decreases above α = 50°. The schlieren photograph shows a bifurcated shock system ahead of the windward fins with a slip line trailing downstream between the fins. A train of disturbances are also seen reflecting between this slip line and the body surface. Strong disturbances from this shock intersection cross the body in almost a perpendicular direction.

At α = 65°, the intersection of the bow shock and the highly curved fin shock has moved well forward of the fins and the near-perpendicular disturbances crossing the body are stronger. Though very difficult to discern, even in the original photograph, a slip line originating at the shock intersection appears to impinge on the windward side of the body just downstream of the body-fin leading-edge juncture. Given the steep slope of the shock waves (the maximum

slope of the fin bow wave at $\alpha = 65°$ was about 78°) and the attendent loss in dynamic pressure behind such a strong shock at Mach 6, it is not surprising that there is a precipitous loss in fin effectiveness as shown in figure 5(b).

The changes in flow patterns discussed above are associated with local flow choking in the vicinity of the windward pair of fins. The phenomenon was first encountered at supersonic speeds and described in reference 7. Reference 8 suggested that the angle of attck for the onset of fin choking was approximately equal to the two-dimensional shock detachment angle at a given Mach number. At Mach 6, shock detachment occurs at 42° and the fact that the loss in fin effectiveness was not encountered until $\alpha > 50°$ probably indicates that other fin-body geometric parameters such as fin leading-edge sweep, aspect ratio, etc. must be involved.

Additional schlieren photographs will be shown subsequently that illustrate how fin deflections significantly affect the choking phenomenon.

Longitudinal performance.- The lift and drag characteristics of the body and body-fin configurations are shown in figure 7. In figure 7(a), both the magnitude and angles of attack for $C_{L_{max}}$ on the isolated body and body with + fins were accurately predicted. This was not the case for the × configuration, figure 7(b), as impact theory consistently underpredicted C_L and C_D. In fact, $C_{L_{max}}$ was underpredicted by at least 10 percent.

Longitudinal stability.- Figure 8(a) shows the longitudinal stability of the isolated body and the + configuration. By reasons of axial symmetry it is assumed that the data for both configurations would pass through the origin. Both theory and experiment show that the longitudinal stability is nonlinear and that the aerodynamic center moves aft as the angle of attack increases.

The stability level of the configuration with the × fins, shown in figure 8(b) was substantially higher than predicted and there was a pitch-up tendency at the highest values of C_N where fin choking was encountered.

Lateral-directional stability.- Figure 9 shows the effect of adding the fins on the lateral-directional characteristics. Modified Newtonian theory predicted the + configuration would be directionally unstable up to about $\alpha = 15°$. In addition, theory predicted the + fins would have a small, but slightly increasing effect on C_{n_β} as the angle of attack increased. The experimental fin contribution, however, was several times greater than that predicted

theoretically; this is believed due primarily to increased q effects in the flow field behind the bow shock on the windward fin. In contrast to the results for the + fins, the theory significantly overestimated the directional contribution of the × fins as shown in figure 9(b). In addition, whereas the theory showed a continuous increase in C_{n_β} with angle of attack, the experimental data increased in magnitude up to $\alpha = 35°$ and then remained essentially constant so that the increment in yawing moment due to the × fins decreased beyond this angle of attack and was negligibly small at $\alpha = 65°$.

Neither fin arrangement produced significant amounts of rolling moment.

Theory predicted the × fins would produce the larger side force increment but experimentally the + fins produced the largest increment in side force.

Longitudinal Trim Characteristics

The effect of control deflection on the longitudinal characteristics of the configuration with the + fins is shown in figure 10(a). For the indicated center of gravity position of 0.5157ℓ, the configuration can be trimmed to an angle of attack of approximately 29° with $\delta_p = -20°$. In general, the aerodynamic center moved aft at higher angles of attack and follows the theoretical trends except for $\delta_p = +10°$ above an angle of attack of 50° where the rate of change in normal, axial, and pitch is reduced. The reason for this is not clear but it may be related to the onset of subsonic flow about the fins and reduced fin lift curve slope.

Trim characteristics with the × fins are shown in figure 10(b). Unlike the more systematic and orderly trends exhibited by the + fins, the × fins show considerable discrepancies with theory, especially at $\delta_p = +10°$ where the configuration exhibits severe pitch up. In addition, large discrepancies occurred between theory and experiment in both normal and axial force.

Schlieren photographs.- Figure 11 shows schlieren photographs of the × fin arrangement with controls deflected +10° and -20°. As noted, the pictures are for -3° sideslip because a complete set was not available at $\beta = 0°$. The small angle of sideslip had only a minor effect on the shock configuration.

Comparing the shock system about the windward fins for the two deflection angles, it can be seen that positive deflections cause a strong, highly curved bow shock ahead of the fins which resulted in the loss in fin effectiveness at high angles of attack and attendent pitch-up seen in the previous figure. At

negative fin deflections the fin shocks are much weaker, the choked flow between the fins is eliminated and fin effectiveness is retained up to the highest angle of attack.

Effect of control deflections on performance.- Figure 12 shows the variation of lift and drag coefficients with angle of attack for various control deflections. For the + fins the magnitudes of C_L and C_D were accurately predicted. A $C_{L_{max}}$ of 5.30 occurred at $\alpha = 50°$ and $\delta_p = +10°$. For the × fin configuration, the predicted values of both C_L and C_D were low. The × fin $C_{L_{max}}$ was 5.65 at $\alpha = 50°$ and $\delta_p = 0°$.

Longitudinal stability.- Figure 13 shows the longitudinal stability of the configuration with various pitch control deflections. Significant discrepancies between thoery and experiment are evident, especially for negative deflections with the + fins (fig. 13(a)) and with all deflections with the × fins, figure 13(b). These data, along with the lift results of the previous figure were used to determine the effect of center of gravity on trimmed lift coefficient. The results are given in figure 14 where it may be noted that for the specified center of gravity of 0.5157ℓ , the + fins produced a trimmed C_L of 2.90 while the × fins developed a $C_{L_{trim}}$ of 3.50.

Although the maximum trimmed C_L for the × fins was higher than for the + fins, this value could not be achieved because the configuration became directionally unstable for a center of gravity aft of 0.5700ℓ. For the + fin orientation, the directional center of gravity for neutral stability was always farther aft than the longitudinal center of gravity. Thus, when trim is considered, there is little difference between the two fin arrangements either in lift attainable or center of gravity position.

Control authority.- Figure 15 compares the control effectiveness of the + and × fins at three typical angles of attack. It is clear from these data that the × fins exhibit essentially twice the control power of the + fins up to the angle of attack where fin choking occurs. Beyond that angle of attack, the two fin orientations provide about the same control power, typified by the results at $\alpha = 60°$.

Pitch control deflection on sideslip derivatives.- Figure 16 shows the effect of pitch control on sideslip derivatives. The isolated panel concept implicit in Newtonian theory predicted negligibly small effects of control

deflection for the + fins (fig. 16(a)). The only difference in C_{n_β}, for example, would be due to the increments in axial force between the windward and leeward fins. Experimentally, the yawing moment derivative for the + fins reached a value three times the predicted value at $\alpha = 65°$. This discrepancy was largely due to interractions of the fin on the body producing yawing moments not accounted for by isolated panel theory.

Theoretically, negative deflections of the × fins produced significant reductions in C_{n_β} because of differences in windward and leeward sideforce and axial force coefficients. The experimental data showed the opposite trend and, generally, failed to follow the theoretical trend as angle of attack increased. The discrepancies in theoretical and experimental C_{n_β} illustrated for the × fins in figure 16(b) clearly show the inadequacies of the theory and point out the complex nature of the flow about the × fins and emphasized the need for further investigations of the body-fin interaction problem with the fins at intermediate roll angles.

Differential control deflection.- Both fin configurations were tested in pitch with controls deflected differentially to obtain rolling moment. It should be emphasized, however, that due to an oversight only the horizontal fins were deflected for the + fin configuration whereas all four fins were deflected in the × configuration. In addition, it is appropriate to note that the computer geometry program employed to describe the deflected fin coordinates (GEMPAK, ref. 9) employs a mirror image concept, that is, only half the vehicle geometry is described. The principal defect with that concept was encountered here with the × fins deflected to produce roll. GEMPAK can not account for that situation, and, indeed can not account for the differential deflections of the horizontal fins in the + orientation. In this case, the isolated fin theoretical data were hand manipulated to obtain roll, yaw and side forces.

It can be seen in figure 17(a) that the theory predicted the value of rolling moment with reasonable accuracy. Yawing moments were grossly under-predicted by factors approaching 4. Similarly, while theory predicted negligible side force values, significant values of C_Y were measured experimentally. Clearly these forces and the resulting yawing moments were due to side loads induced on the body by the fins and not accounted for theoretically by isolated panel methods.

As a result of the problems encountered with GEMPAK, no theory results are

shown in figure 17(b) for the × fin arrangement. In addition, because of the oversight mentioned previously, the data for the two fin arrangements are not comparable. The large variations of lateral-directional parameters with angle of attack for the × fin orientation, figure 17(b), were due to the cumulative effects of the complex flow phenomena alluded to earlier, such as shielding, choking, separation, shock impingement, cross flows, and so forth. In any event, impact theory methods would not account for these effects.

CONCLUSIONS

An experimental and theoretical study was conducted to determine the stability and performance characteristics of a finned cylindrical body at Mach 6. The model had a simple cylindrical fuselage and a 12°/6° biconic nose. Component build up and control deflection results led to the following conclusions:

1. Forces and moments could be accurately predicted on the configuration with the + fins using modified Newtonian theory on the windward surfaces of the body and fins and a Prandtl-Meyer expansion from freestream on the leeward surfaces.
2. Serious discrepancies occurred between theory and experiment when the fins were in the × orientation where, below $\alpha = 50°$, the theory underpredicted the fin contribution by 50 percent.
3. Above an angle of attack of 50°, the × fin contribution to lift and pitching moment diminished percipitiously as a result of local flow choking between the body and the windward fins.
4. Fin deflection had a large effect on the occurrance of the choking phenomena with negative deflections tending to alleviate the problem and positive deflections exacerbating the effects to the extent that pitch up occurred at high angles of attck.
5. Theory accurately predicted the maximum lift coefficient for the + fin arrangement and the angle of attack at which it occurred.
6. Maximum lift coefficient with × fins was underpredicted by at least 10 percent.
7. The + configuration exhibited increasingly positive directional stability at angle of attack with values about three times that of the × configuration.
8. The × fins had about double the control authority in pitch as the +

fins up to the angle of attack for onset of fin choking.

9. The maximum attainable lift for the × finned arrangement was about 14 percent higher than for the + fin arrangement but this trimmed lift was unusable because the configuration became directionally unstable. Thus, when directional stability was taken into consideration, both fin arrangements produced about the same trimmed lift coefficient of about 5.20.

REFERENCES

1. Penland, J. A.: Aerodynamic Force Characteristics of a Series of Lifting Cone and Cone-Cylinder Configurations at a Mach Number of 6.83 and Angles of Attack up to 130°. NASA TN D-840.

2. Landrum, E. J.; and Babb, C. D.: Wind-Tunnel Force and Flow-Visualization Data at Mach Numbers From 1.6 to 4.63 for a Series of Bodies of Revolution at Angles of Attack From -4° to 60°. NASA TM-78813, 1979.

3. Landrum, E. J.: Wind-Tunnel Pressure Data at Mach Numbers From 1.6 to 4.63 for a Series of Bodies of Revolution at Angles of Attack From -4° to 60°. NASA TM X-3558, October 1977.

4. Wardlaw, A. B., Jr.; Baltakis, F. P.; Soloman, J. L.; and Hackerman, L. B.: An Inviscid Computational Method for Tactical Missile Configurations. NSWC TR 81-457, 1981.

5. Gentry, A. E.; and Smyth, D. N.: Hypersonic Arbitrary-Body Aerodynamic Computer Program (Mark III Version). Report DAC 61552, Vols. I and II, April 1968.

6. Johnston, P. J.; and Hartman, E. R.: Experimental and Theoretical Performance and Stability of an Airbreathing Missile Concept at Mach Numbers From 3.5 to 6.0. NASA TP-2647, 1986.

7. Stallings, R. L., Jr.; Lamb, M.; and Watson, C. B.: Effect of Reynolds Number on Stability Characteristics of a Cruciform Wing-Body at Supersonic Speeds. NASA TP-1683, July 1980.

8. Stallings, R. L., Jr.: Reynolds Number Effects on Aerodynamic Characteristics at Large Angles of Attack. AIAA Paper 79-0301R.

9. Stack, S. H.; Edwards, C. L. W.; and Small, W. J.: GEMPAK: An Arbitrary Aircraft Geometry Generator. NASA TP-1022, August 1977.

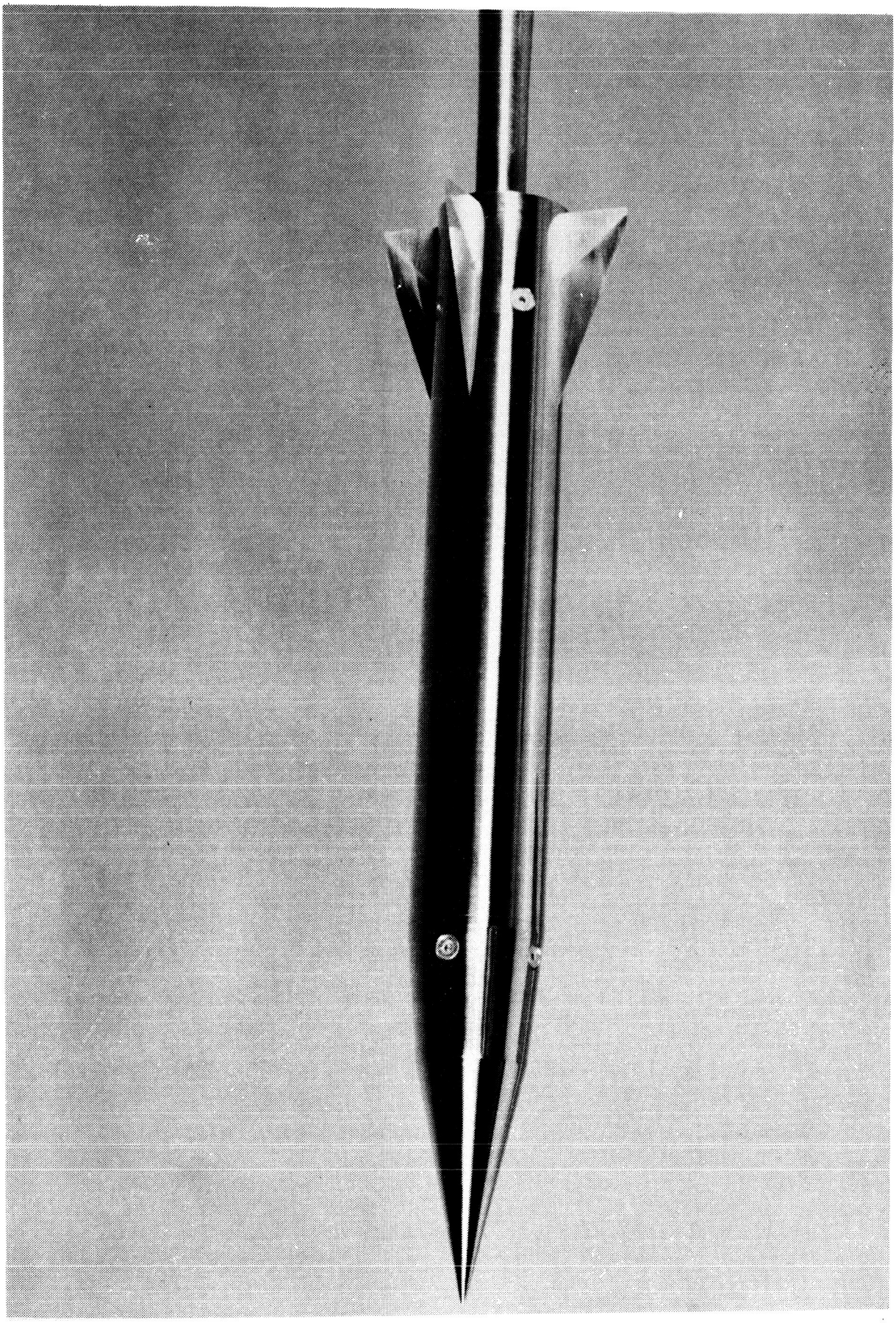

Figure 1. - Photograph of model.

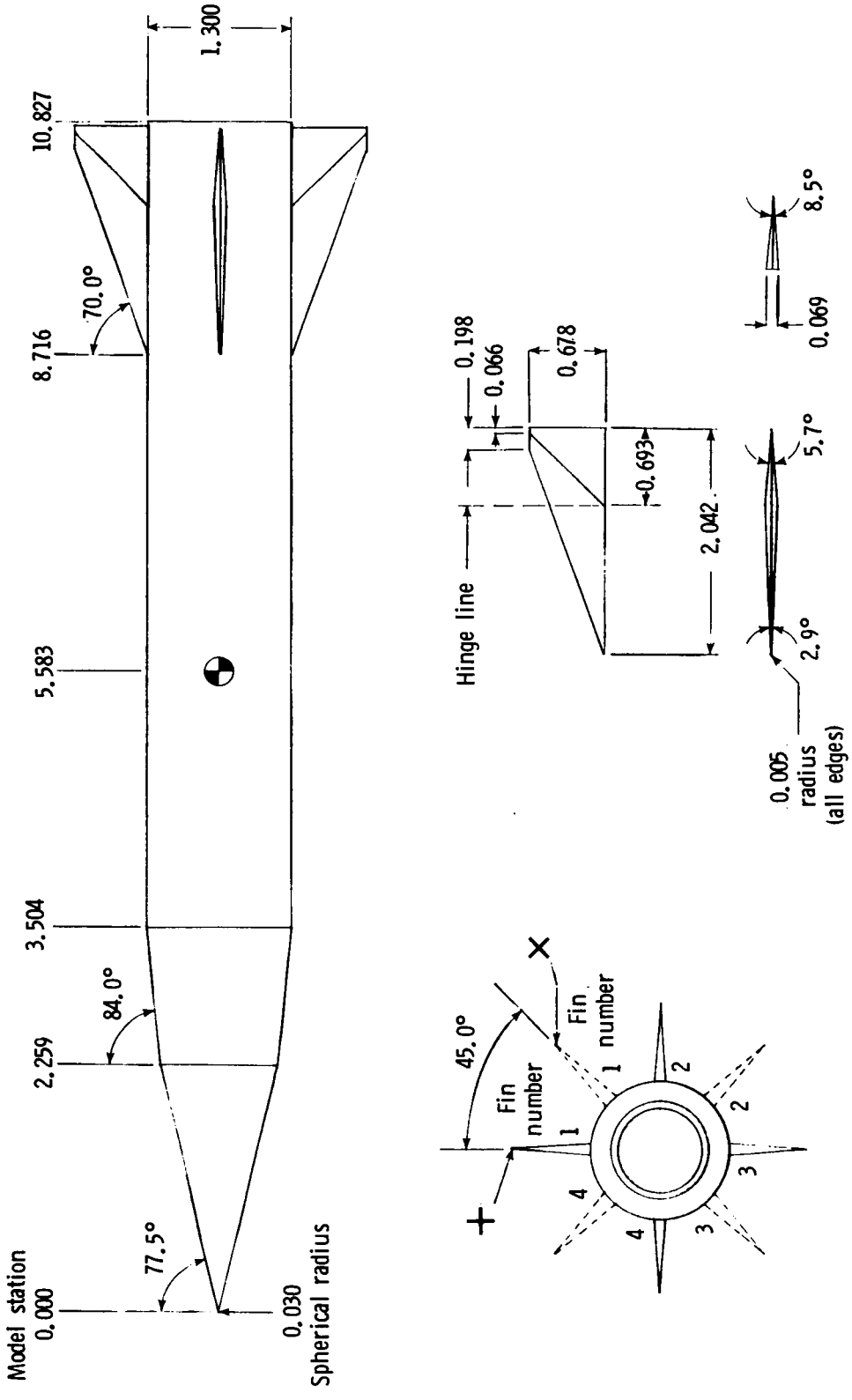

Figure 2. - Details of model. All linear dimensions in inches.

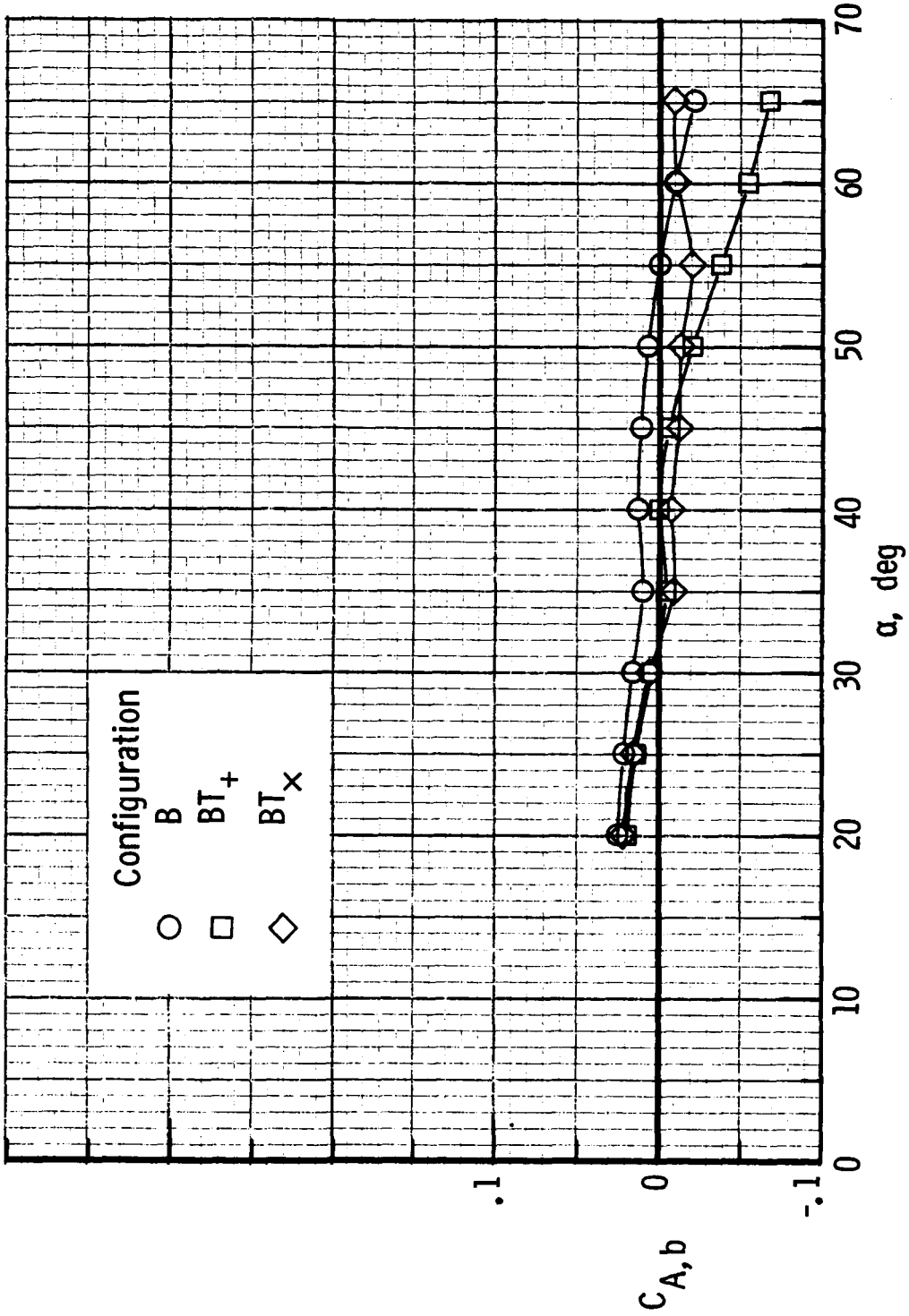

Figure 3. - Representative base axial-force coefficients for $\delta_p = 0^0$.

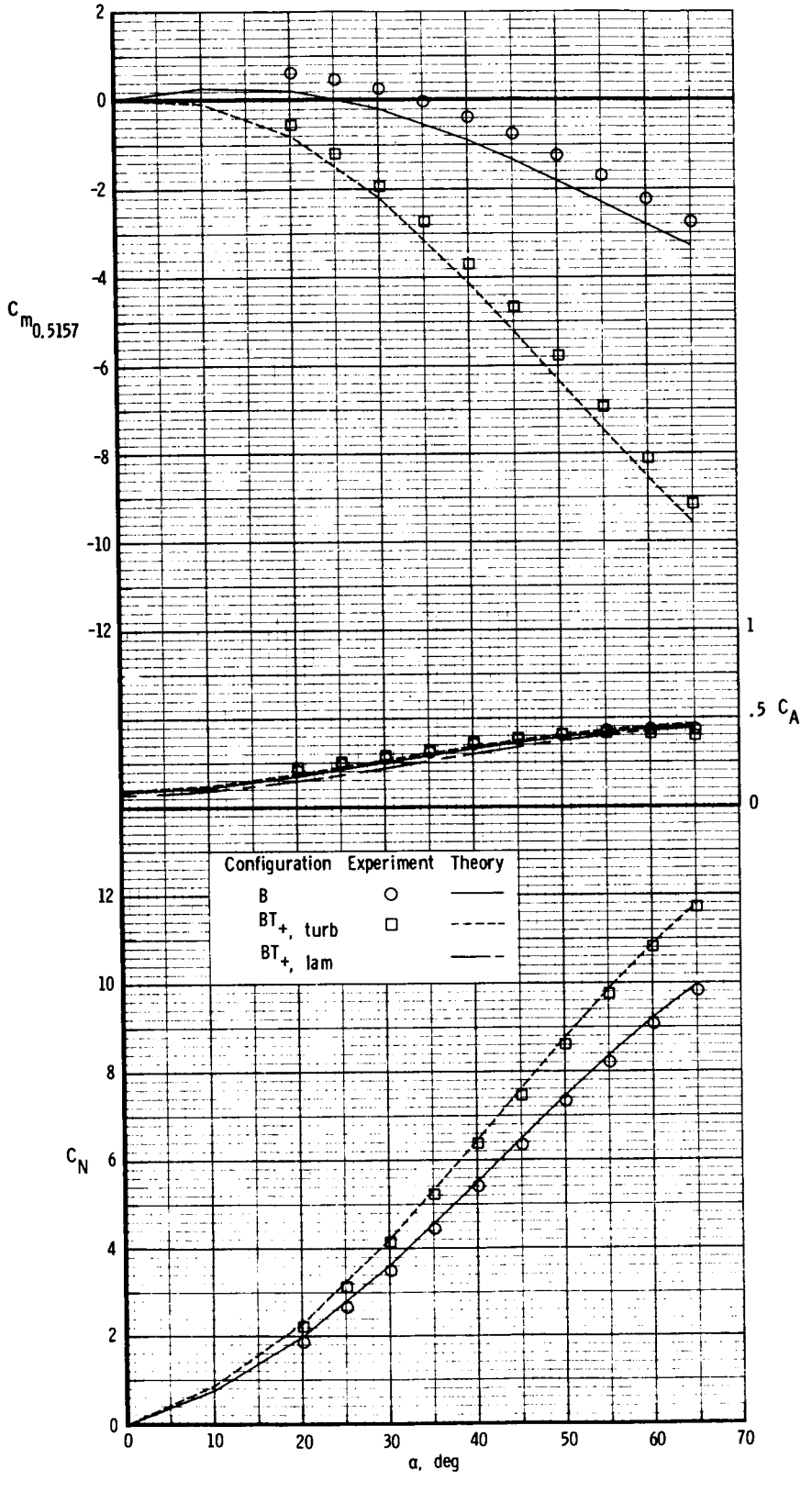

(a) + fins.

Figure 4. - Effect of component build-up on longitudinal aerodynamic characteristics for $\delta_p = 0°$.

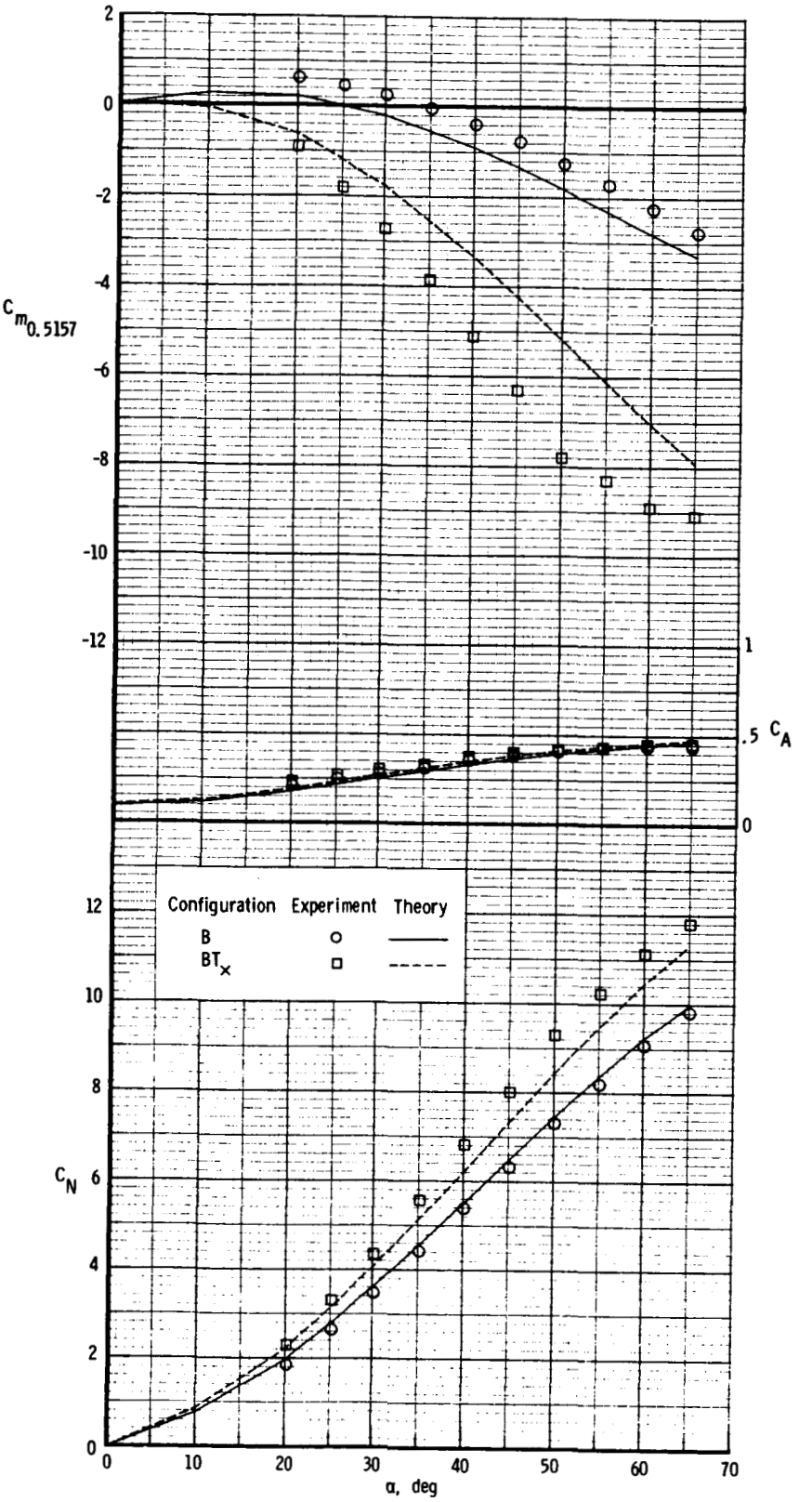

(b) x fins.

Figure 4. - Concluded.

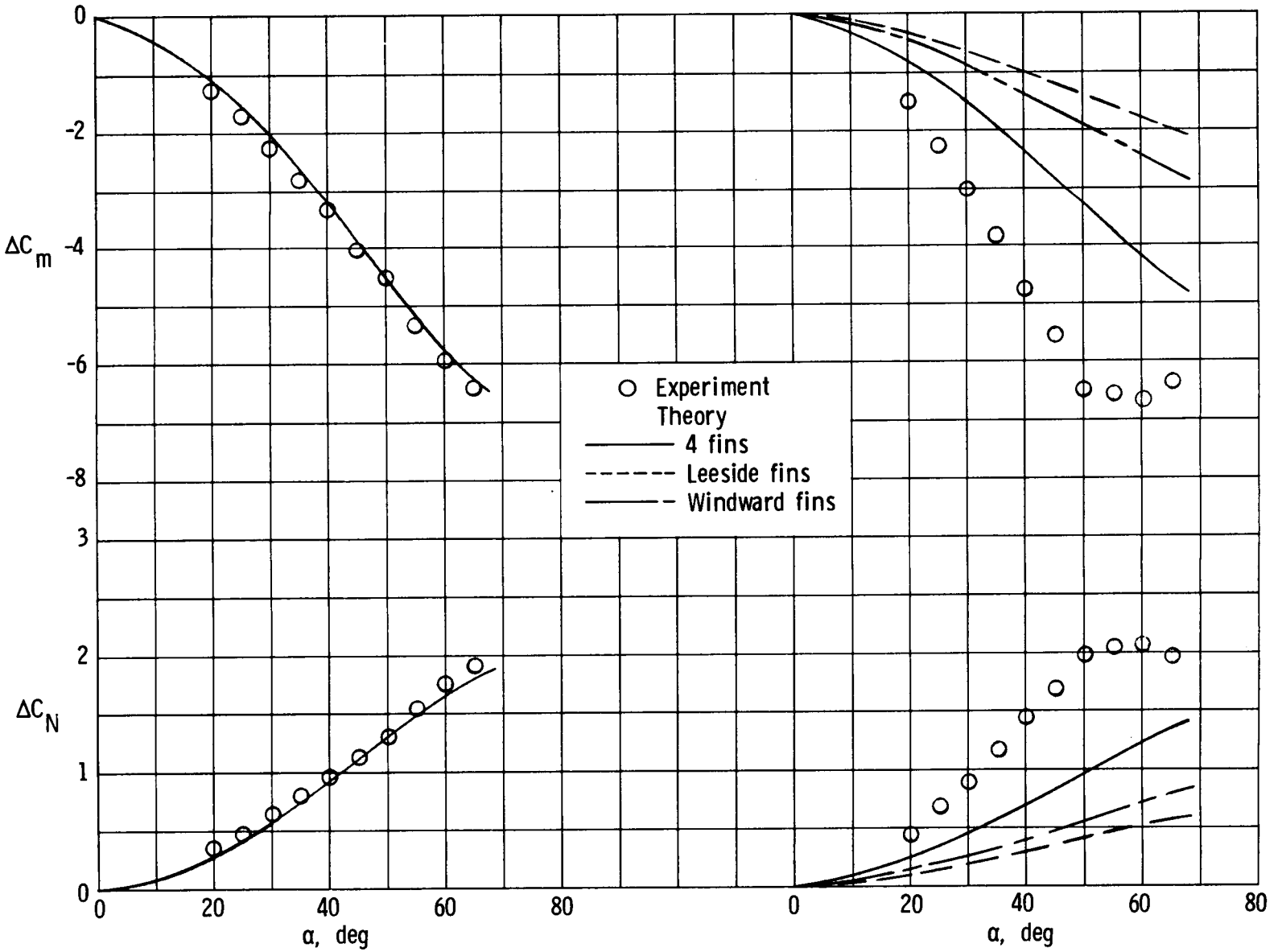

(a) + fins.

(b) x fins.

Figure 5. - Incremental fin contribution on longitudinal aerodynamic characteristics for $\delta_p = 0^0$.

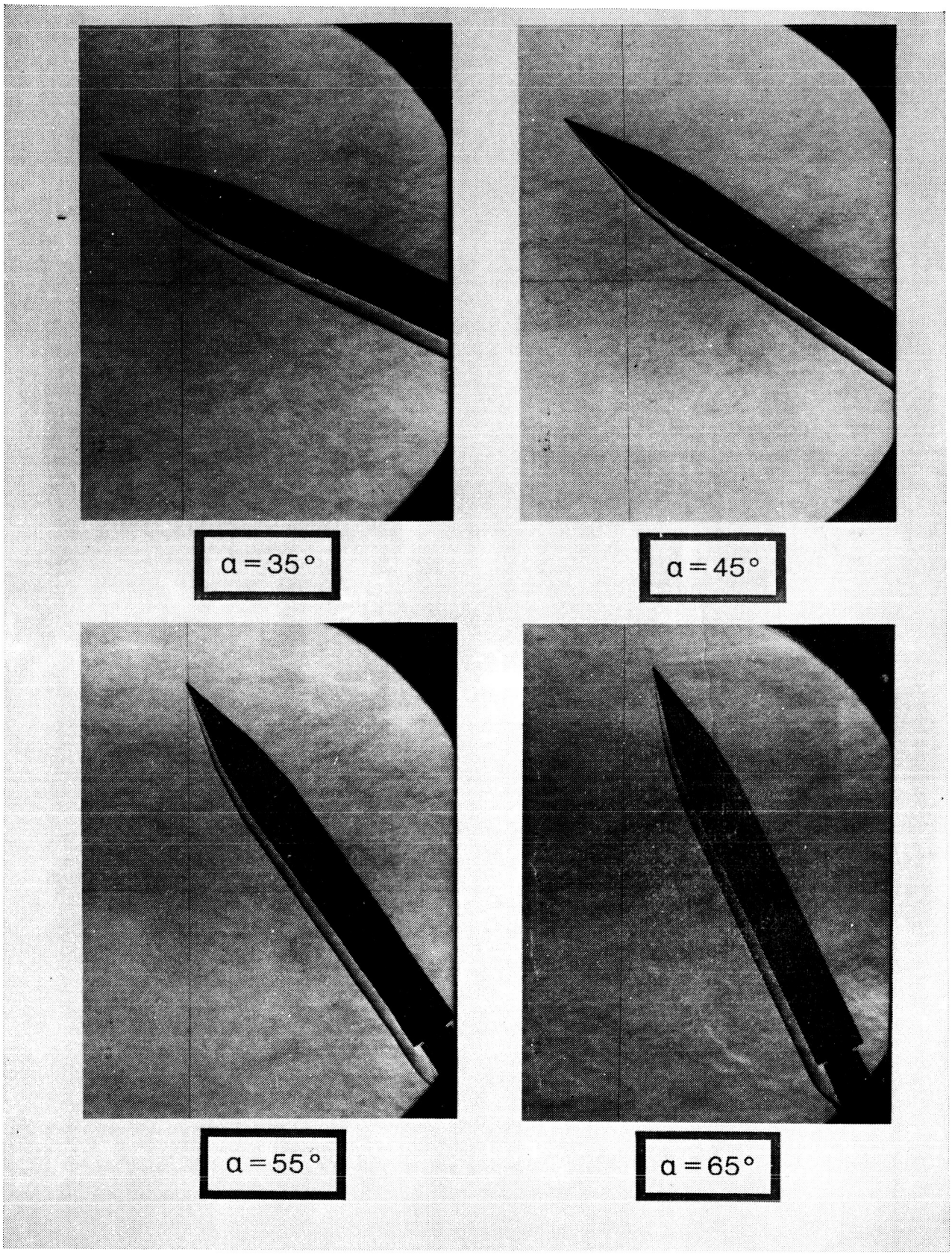

(a) Body alone.

Figure 6. - Schlieren photographs of various configurations.

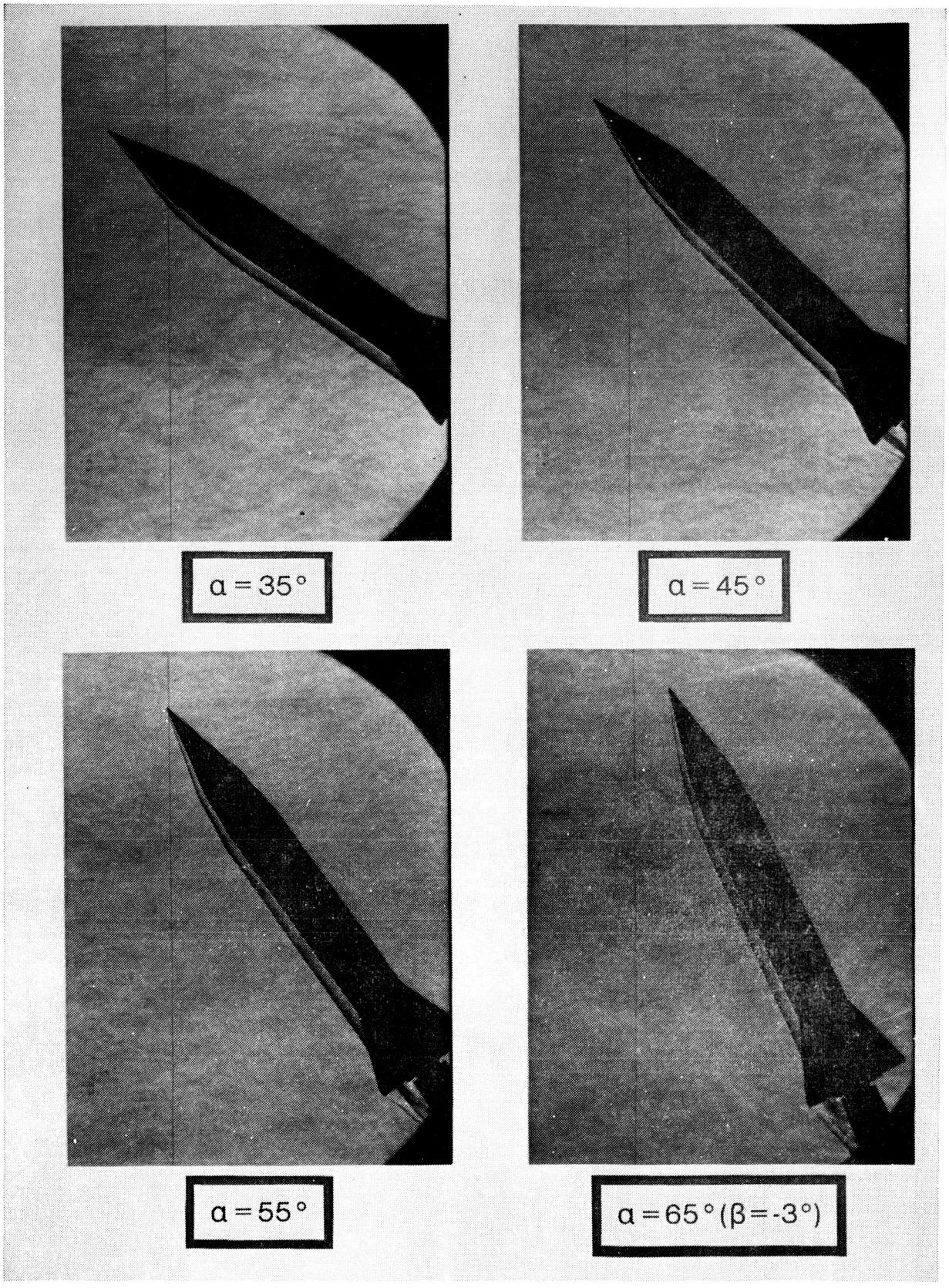

(b) + fins, δ_p = 0°.

Figure 6. - Continued.

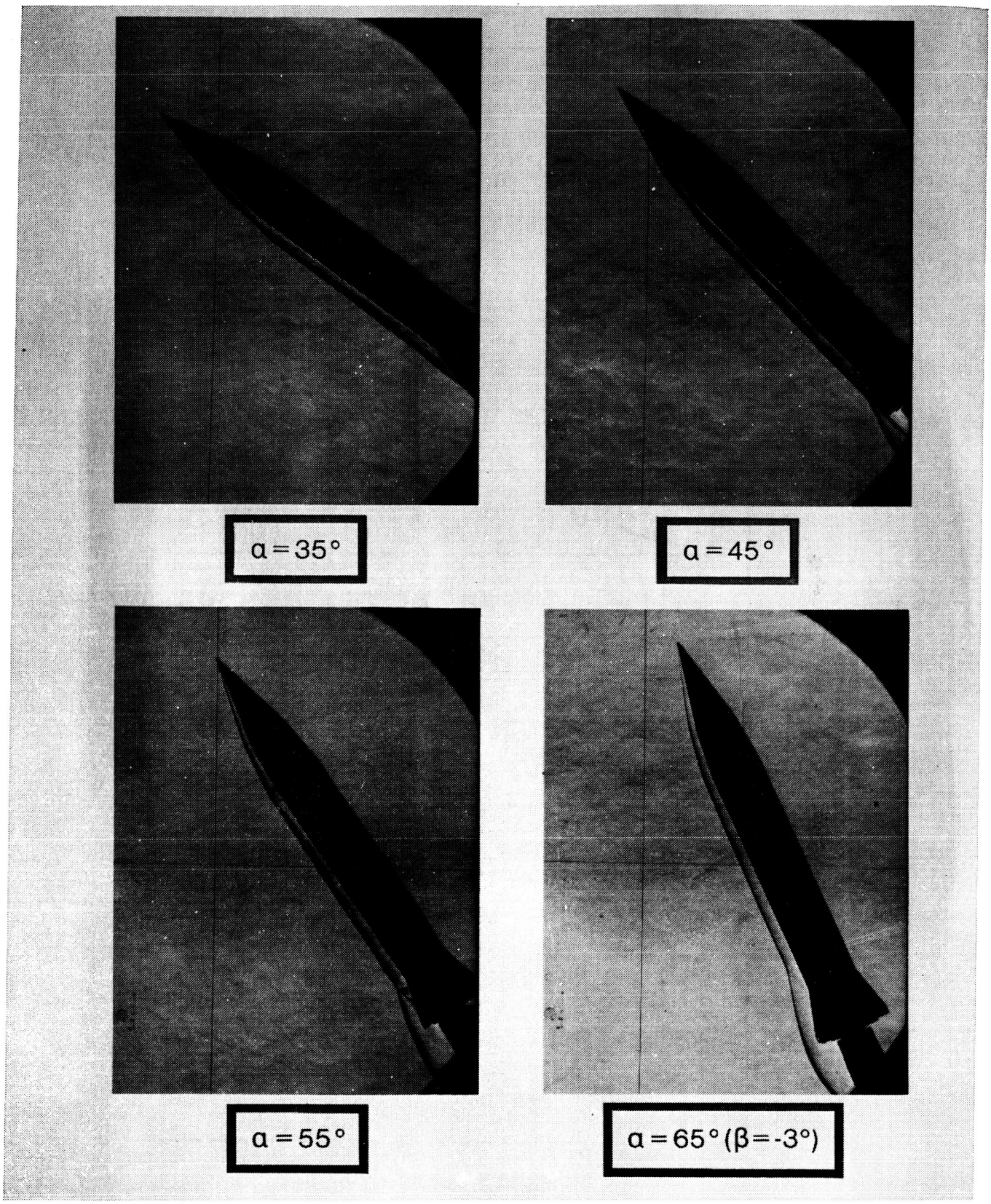

(c) x fins, $\delta_p = 0°$.

Figure 6. - Concluded.

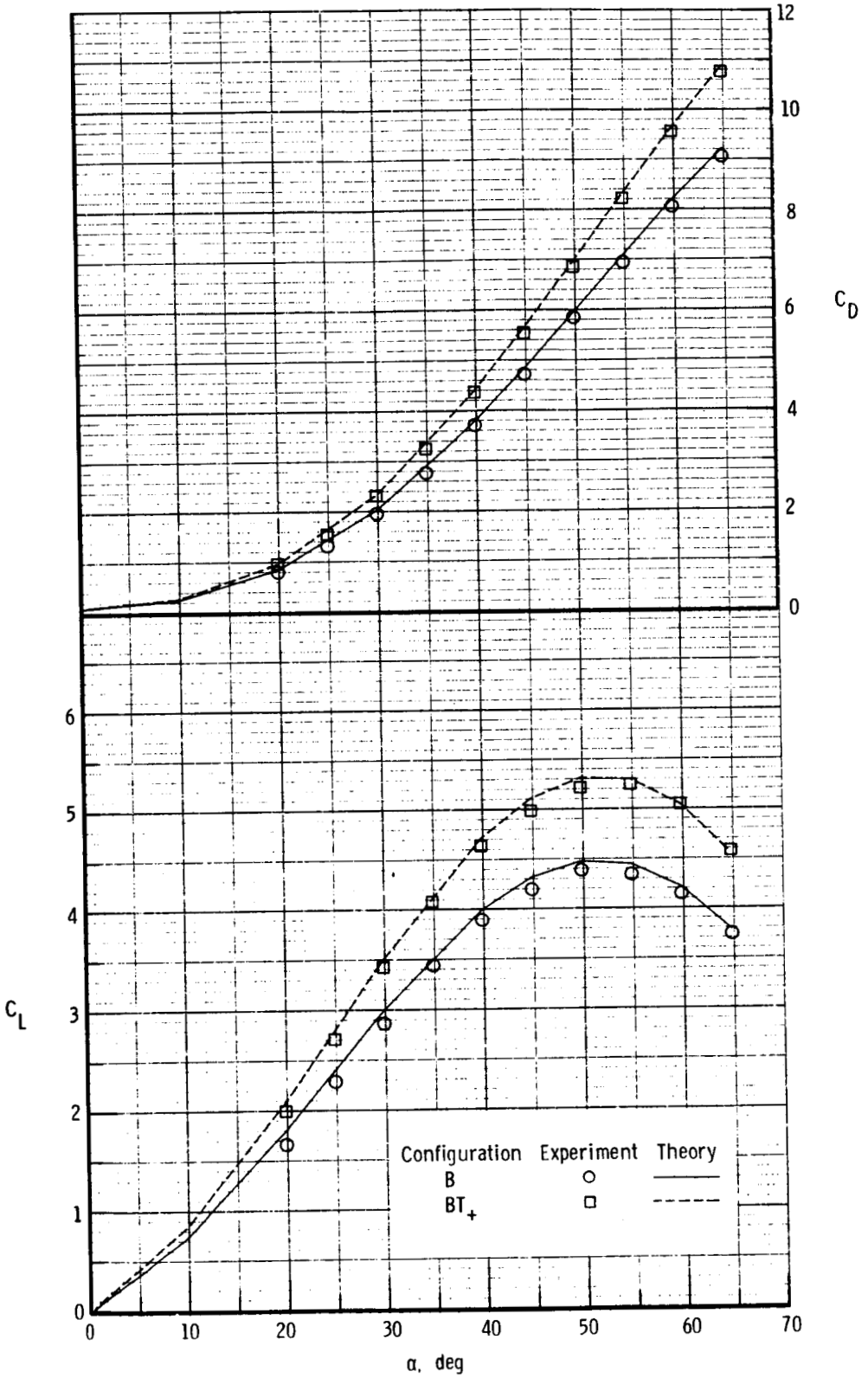

(a) + fins.

Figure 7. - Effect of component build-up on performance characteristics for $\delta_p = 0^0$.

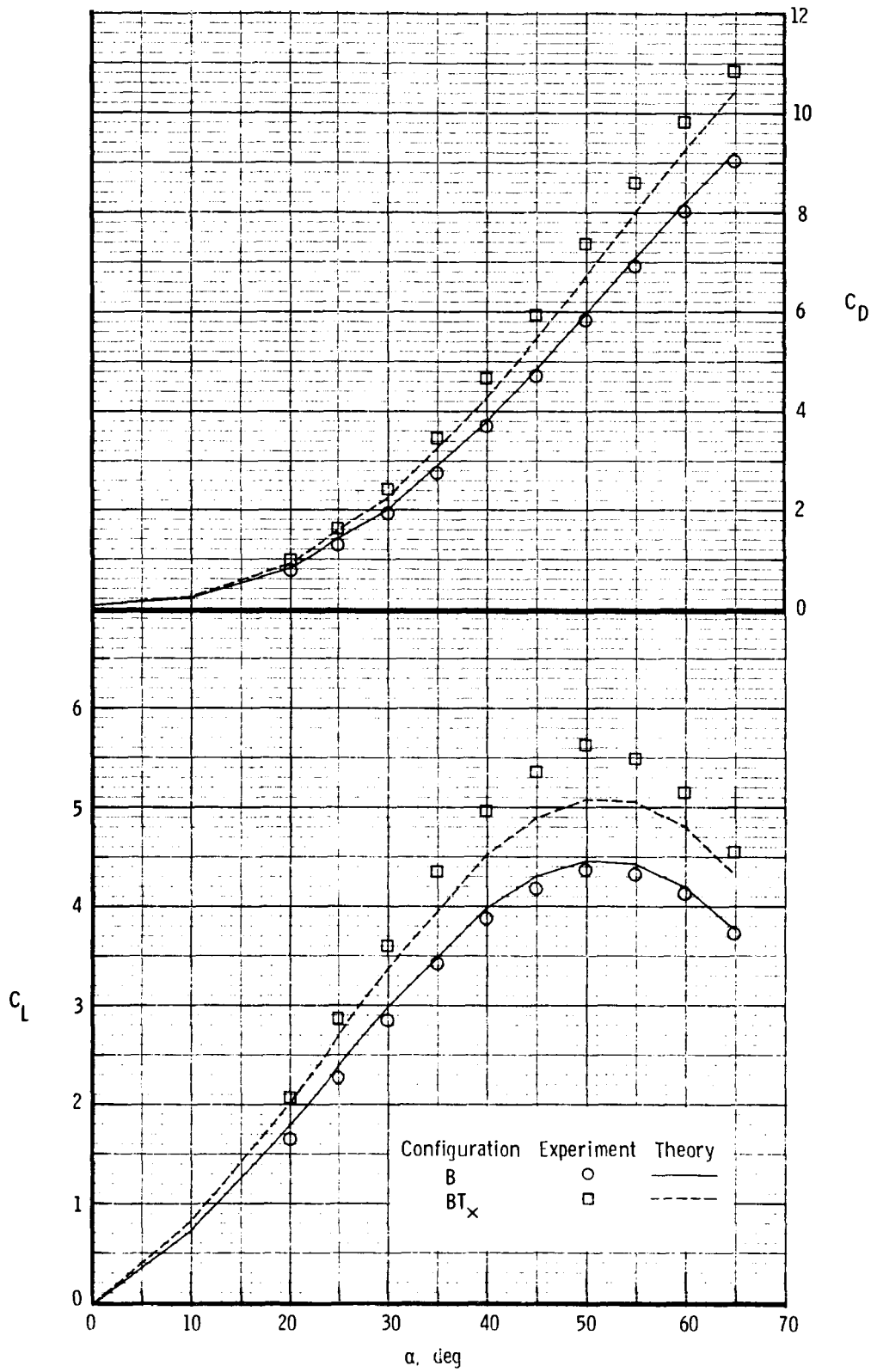

(b) x fins.

Figure 7. - Concluded.

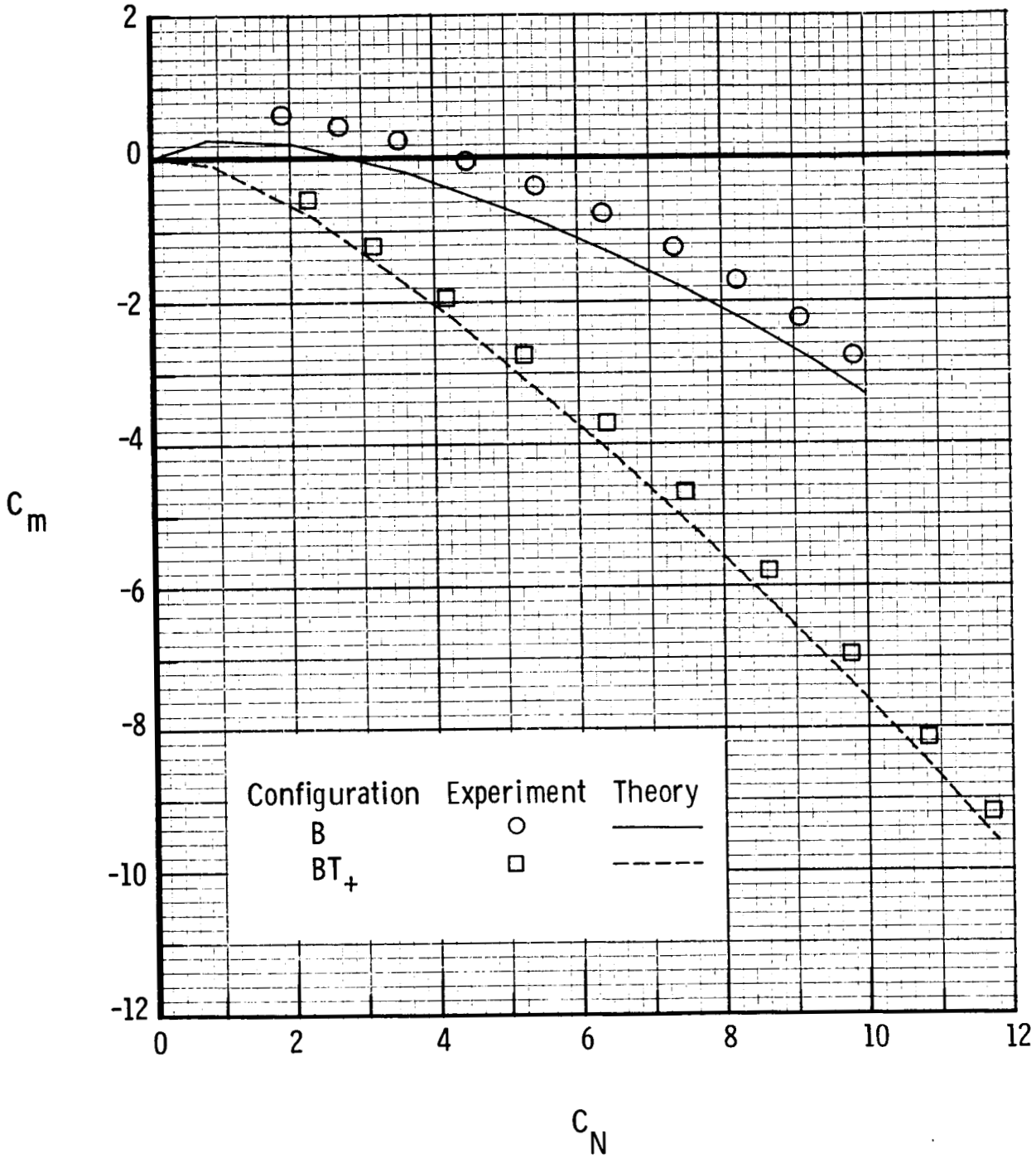

(a) + fins.

Figure 8. - Effect of component build-up on longitudinal stability for $\delta_p = 0^0$.

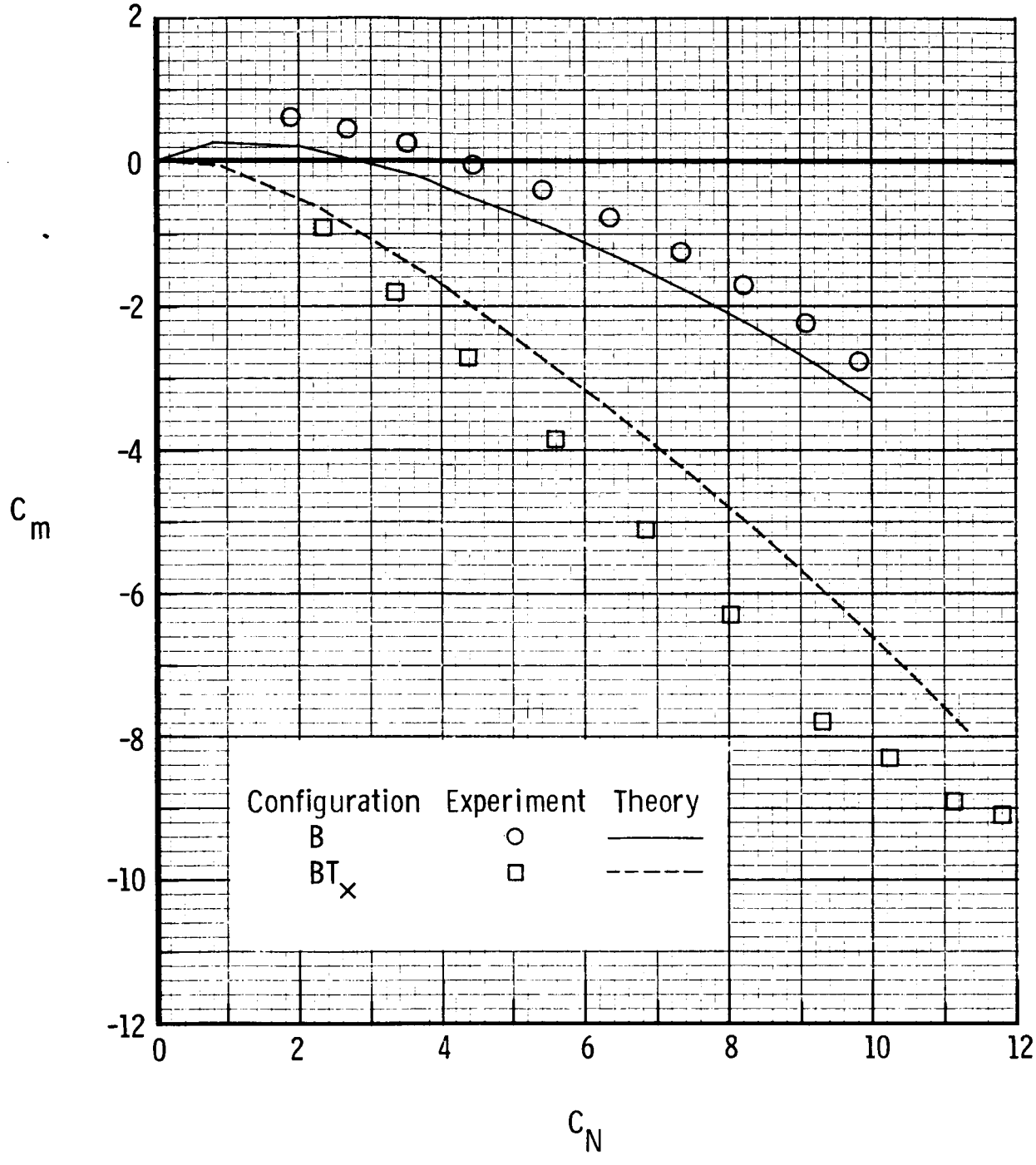

(b) x fins.

Figure 8. - Concluded.

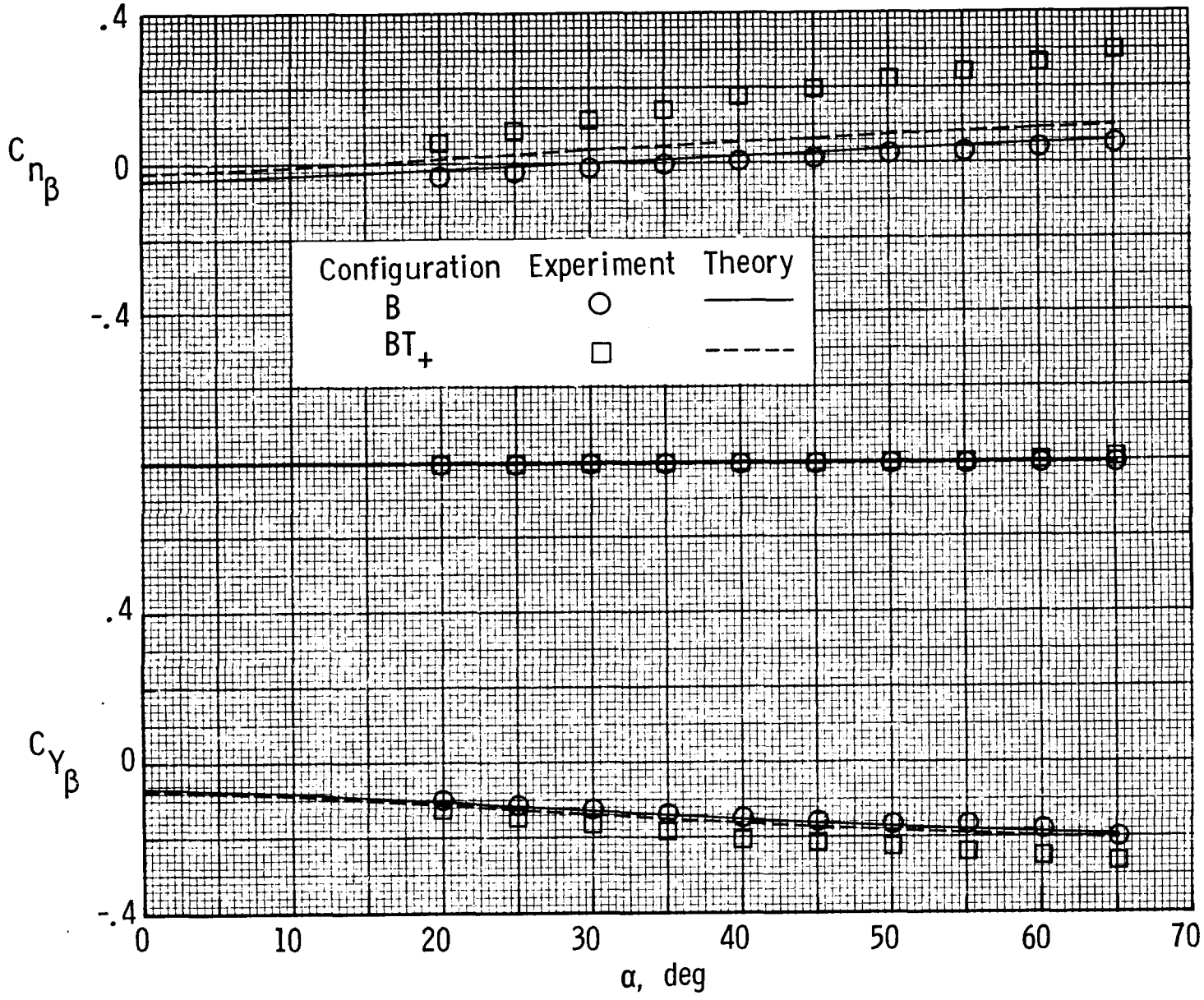

(a) + fins.

Figure 9. - Effect of component build-up on sideslip derivatives for $\delta_p = 0^0$.

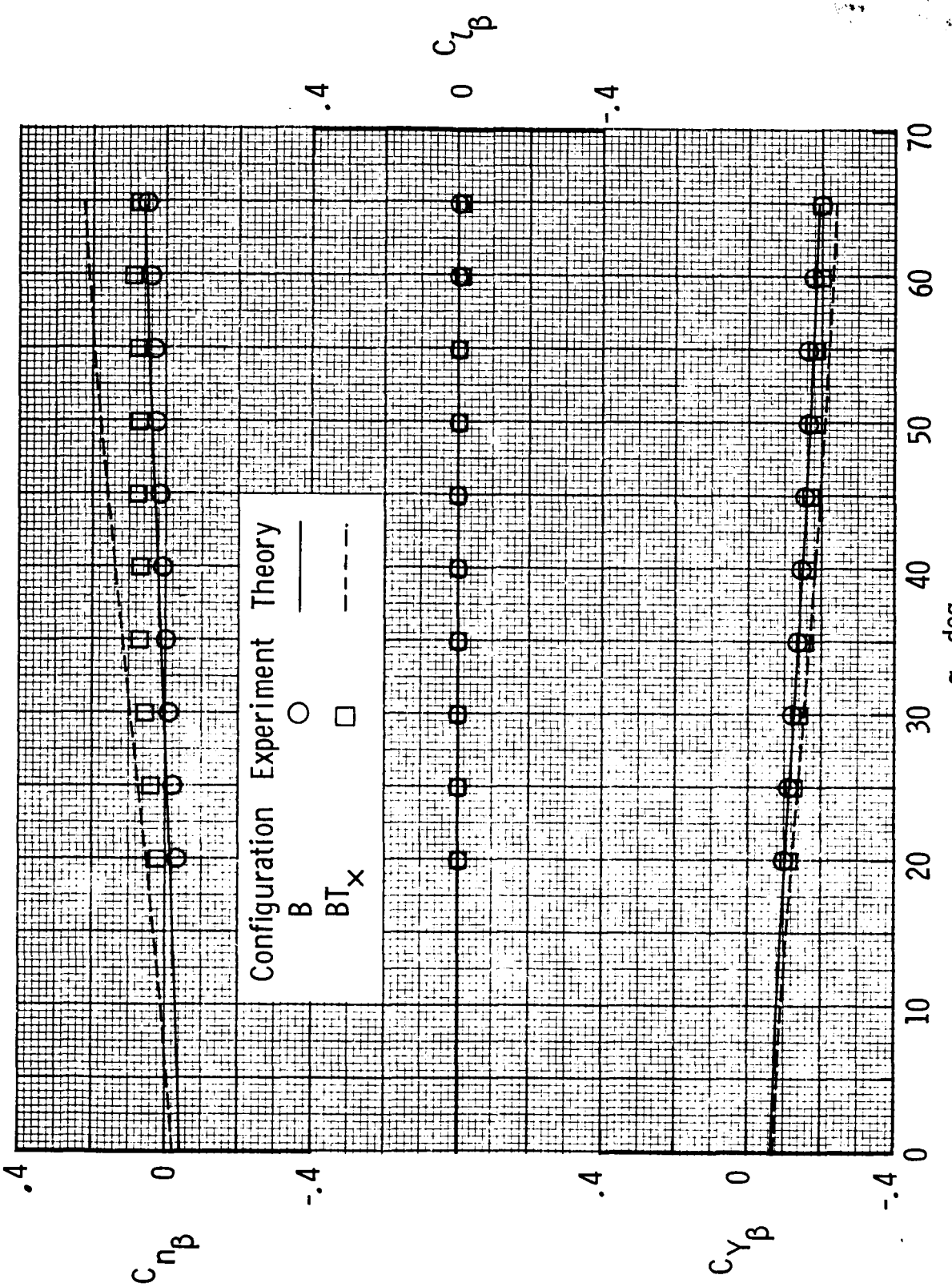

(b) x fins.

Figure 9. - Concluded.

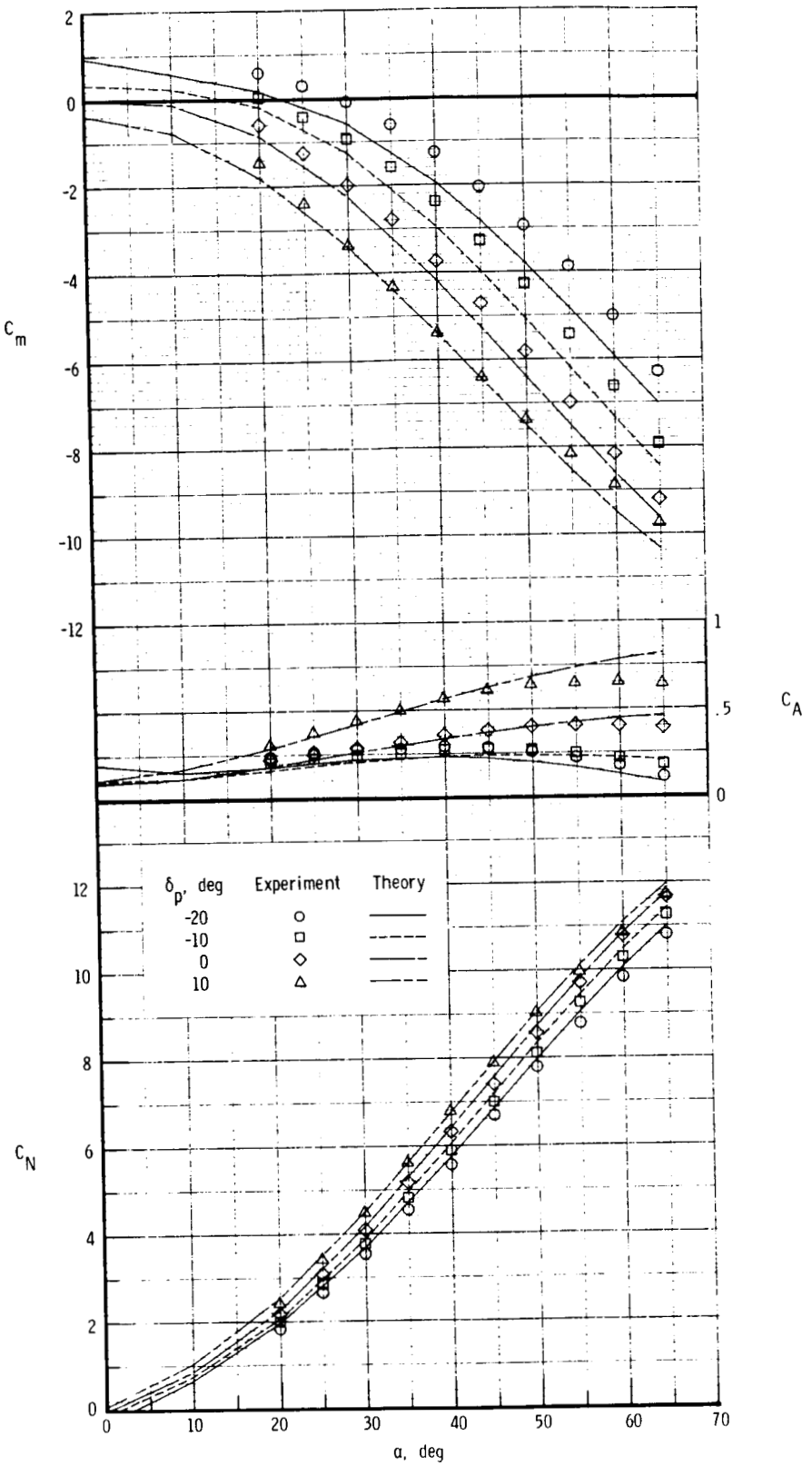

(a) + fins.

Figure 10. - Effect of pitch-control deflection on longitudinal aerodynamic characteristics.

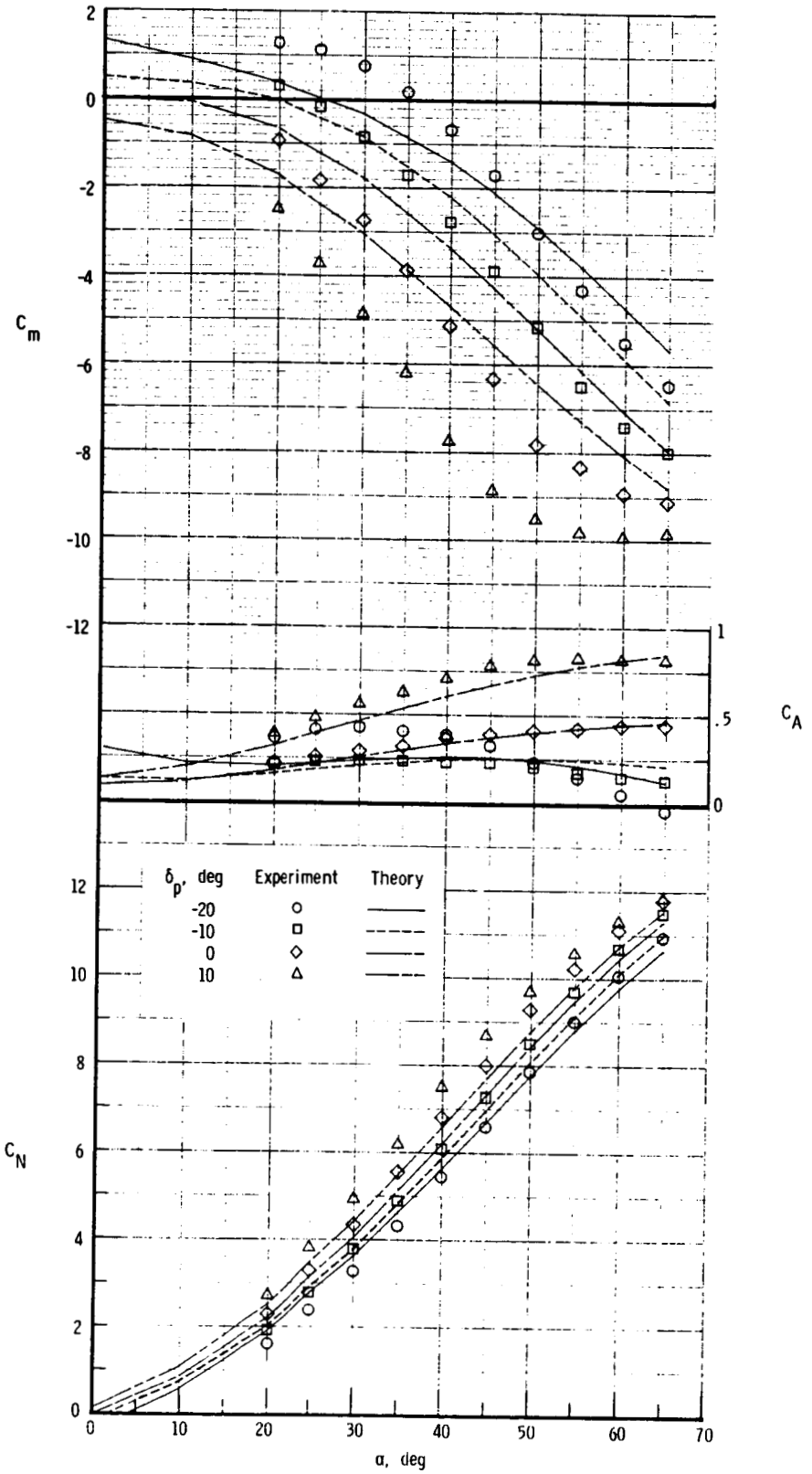

(b) x fins.

Figure 10. - Concluded.

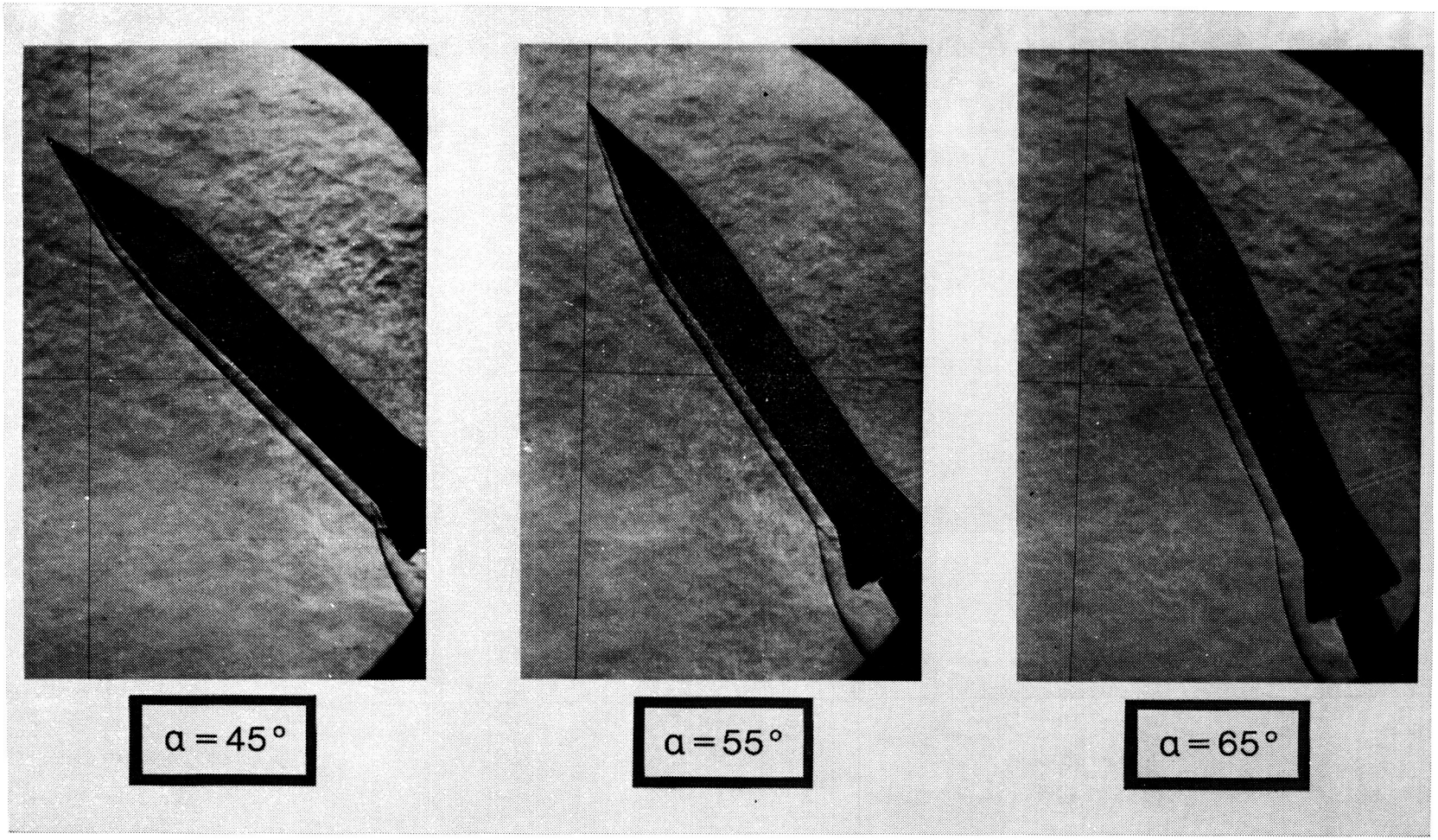

(a) x fins, δ_p = 10°.

Figure 11. - Schlieren photographs of choking and other phenomena (β = -3°).

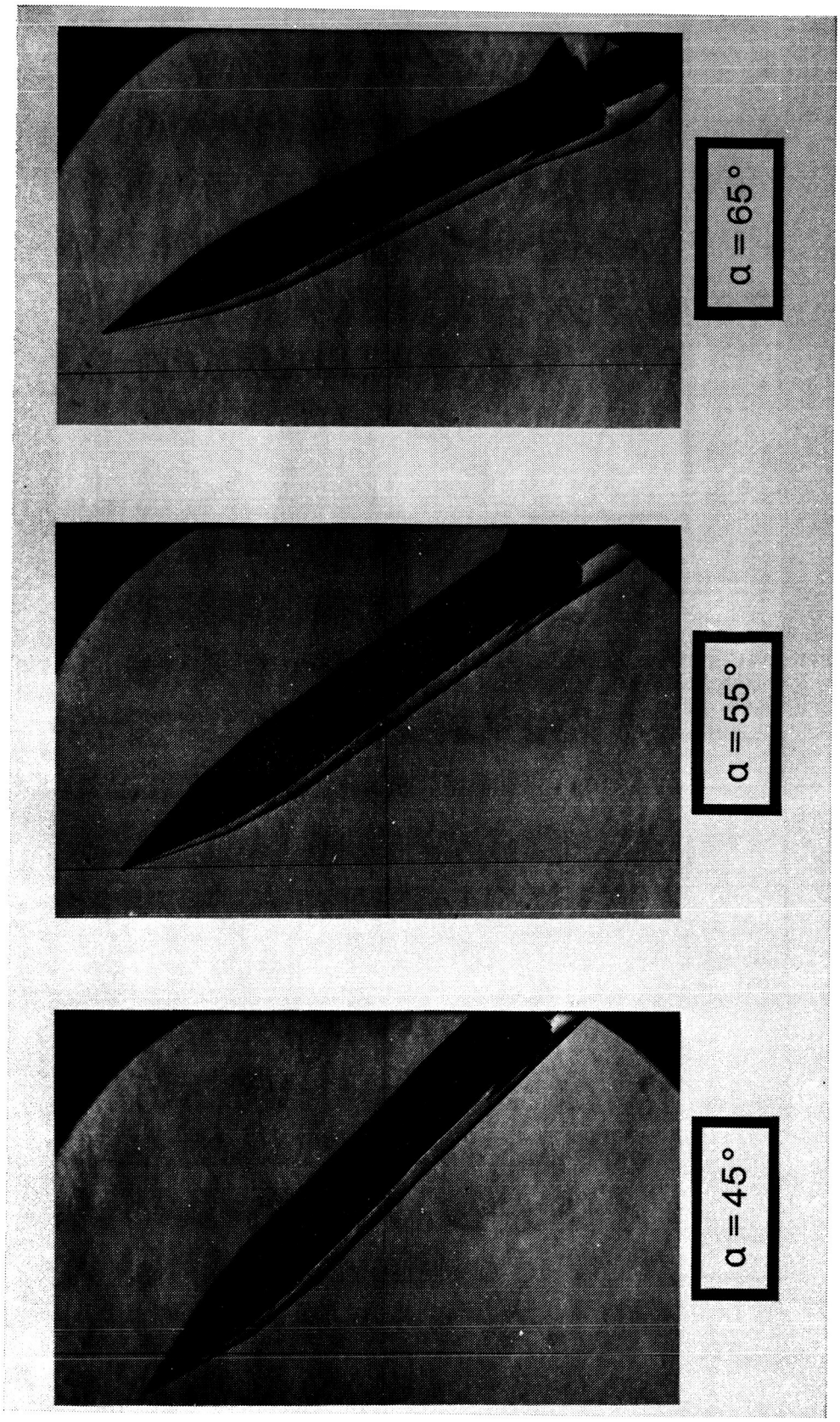

(b) x fins, δ_p = -20°.

Figure 11. - Concluded.

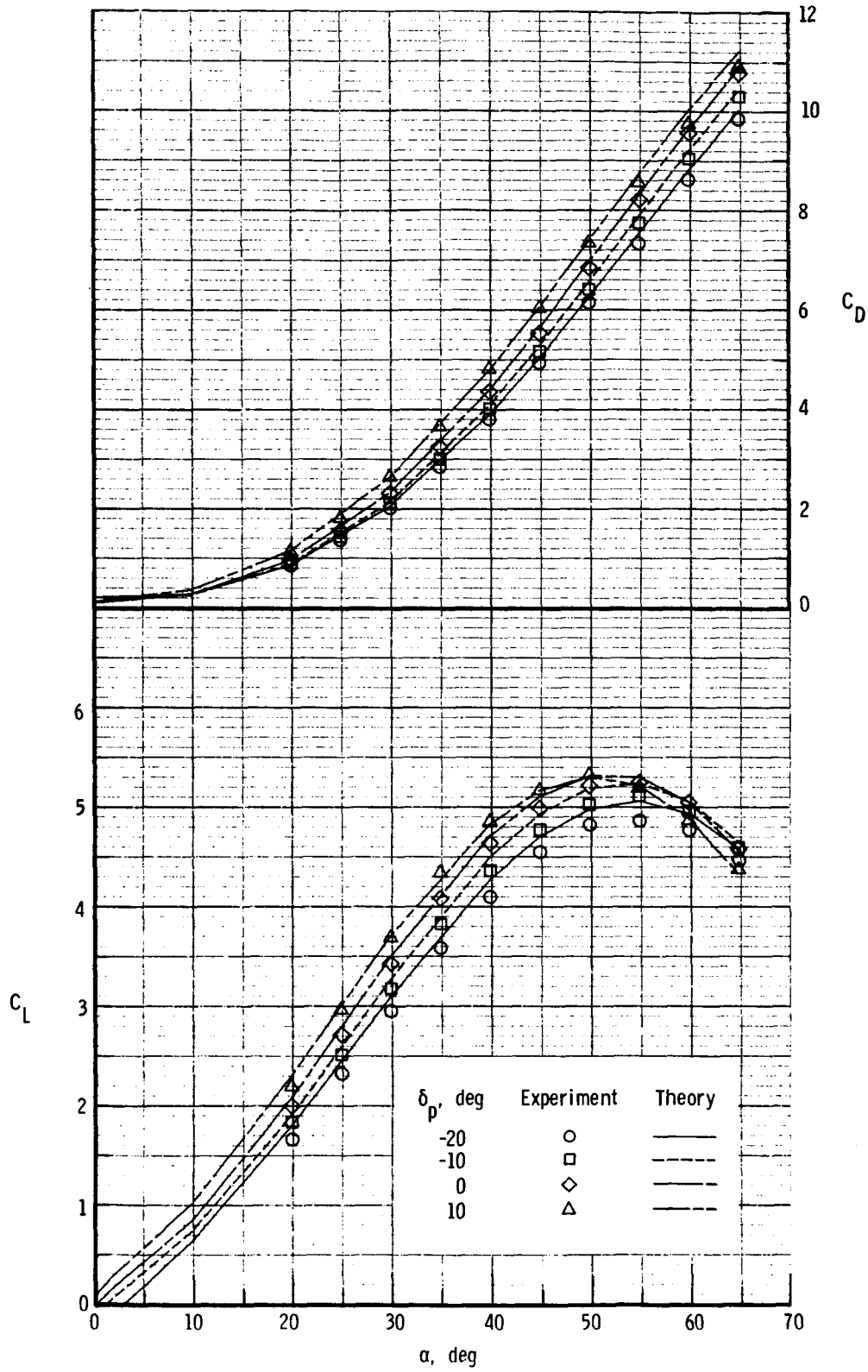

(a) + fins.

Figure 12. - Effect of pitch-control deflection on performance characteristics.

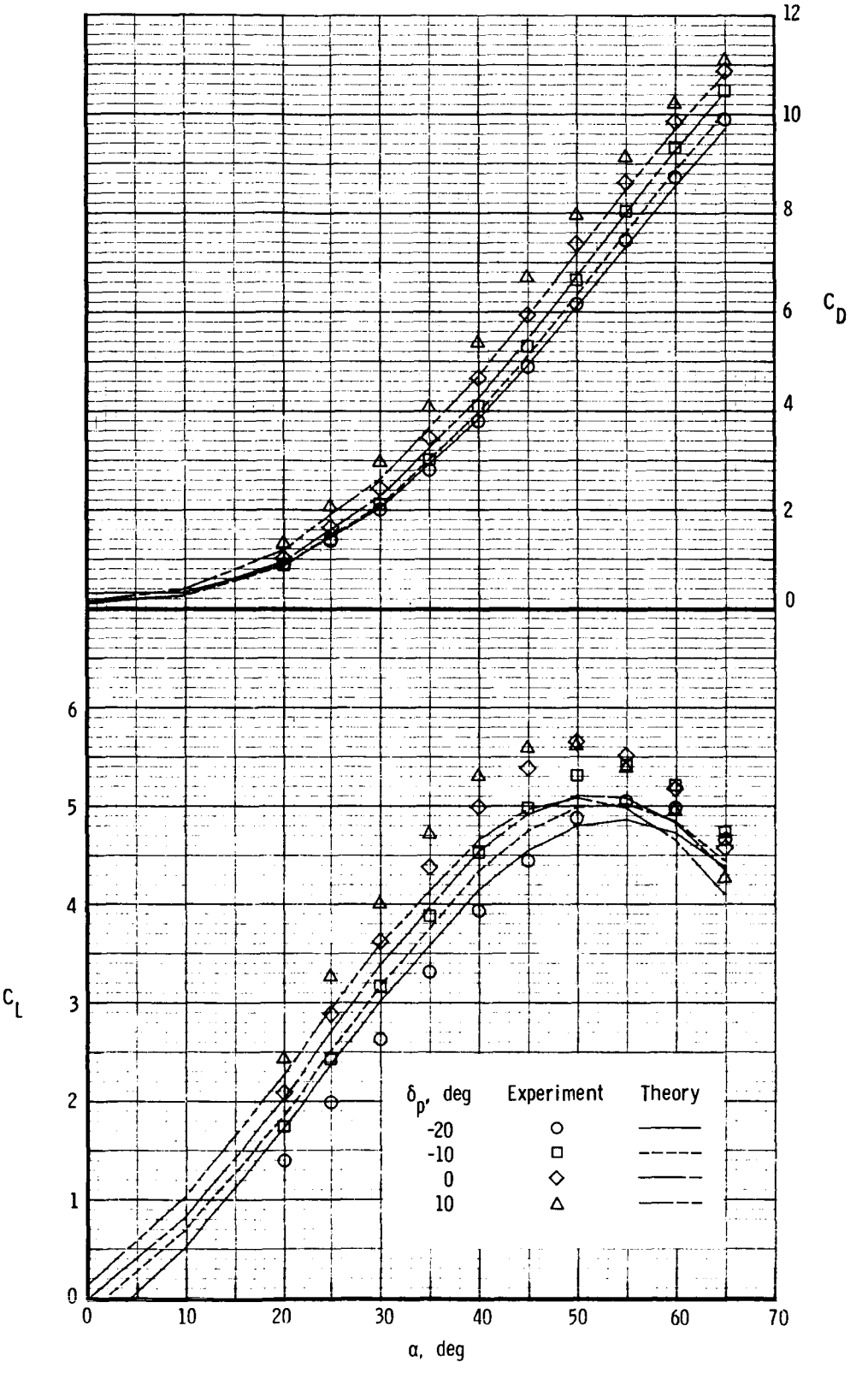

(b) x fins.

Figure 12. - Concluded.

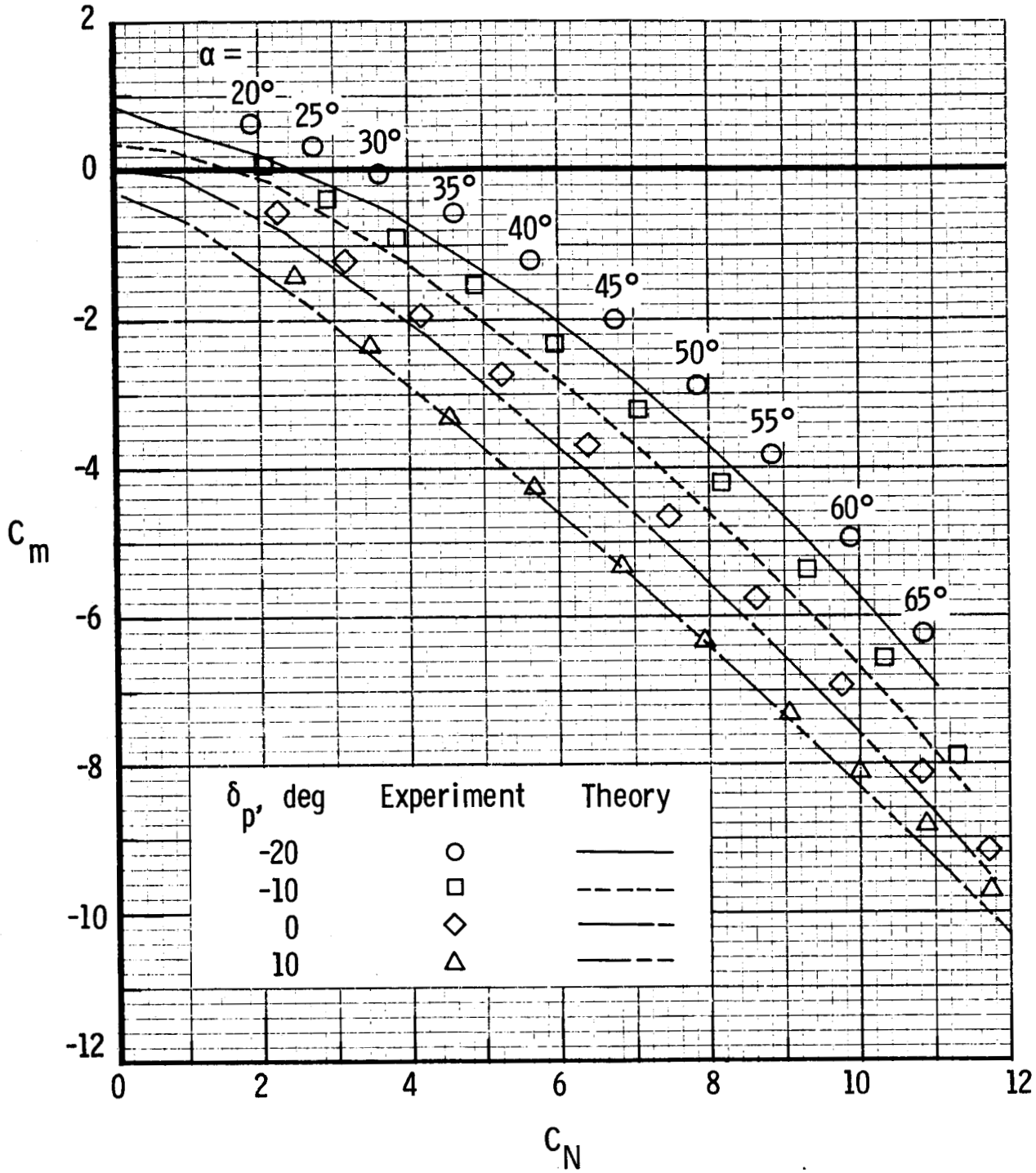

(a) + fins.

Figure 13. - Effect of pitch-control deflection on longitudinal stability.

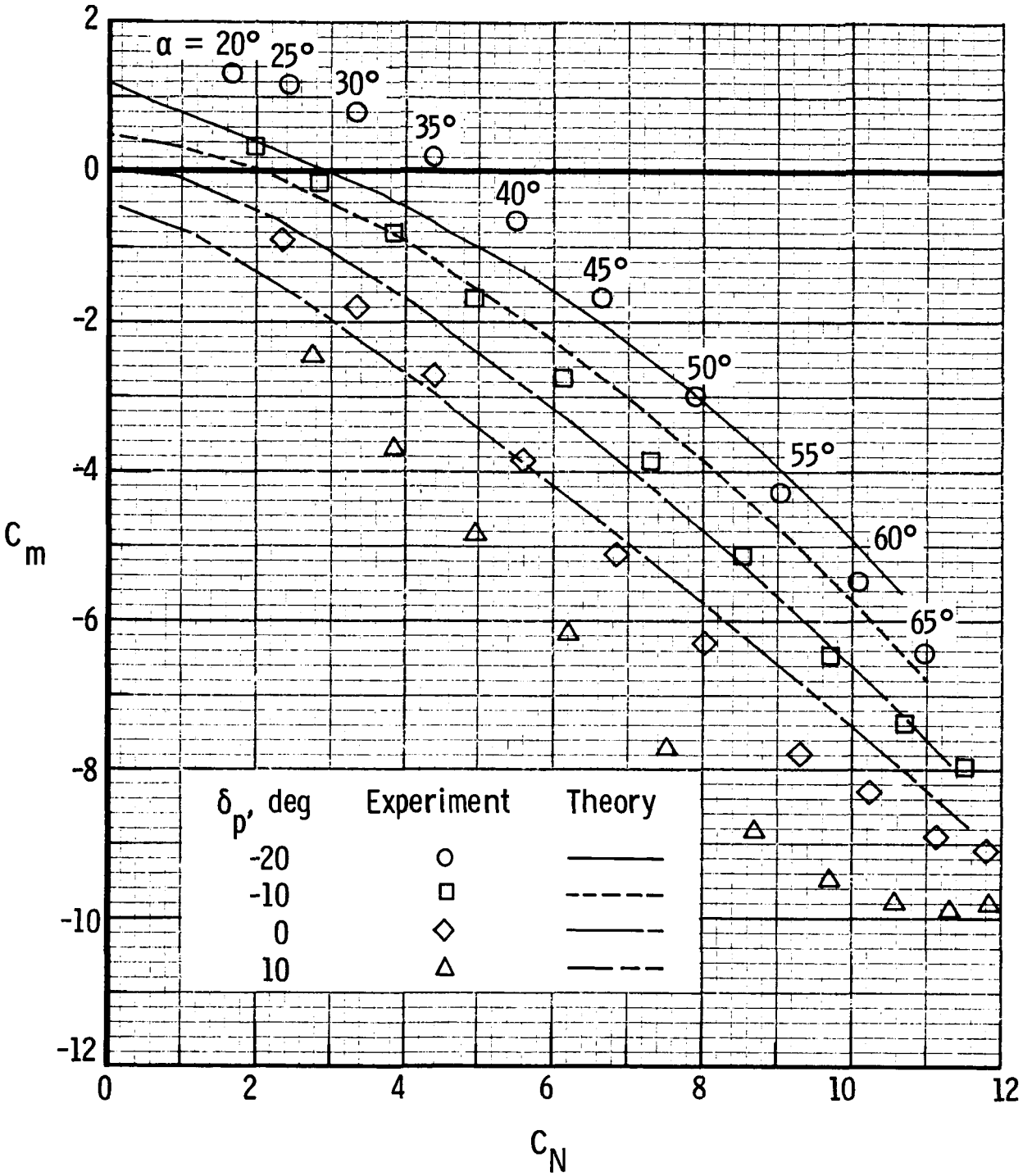

(b) x fins.

Figure 13. - Concluded.

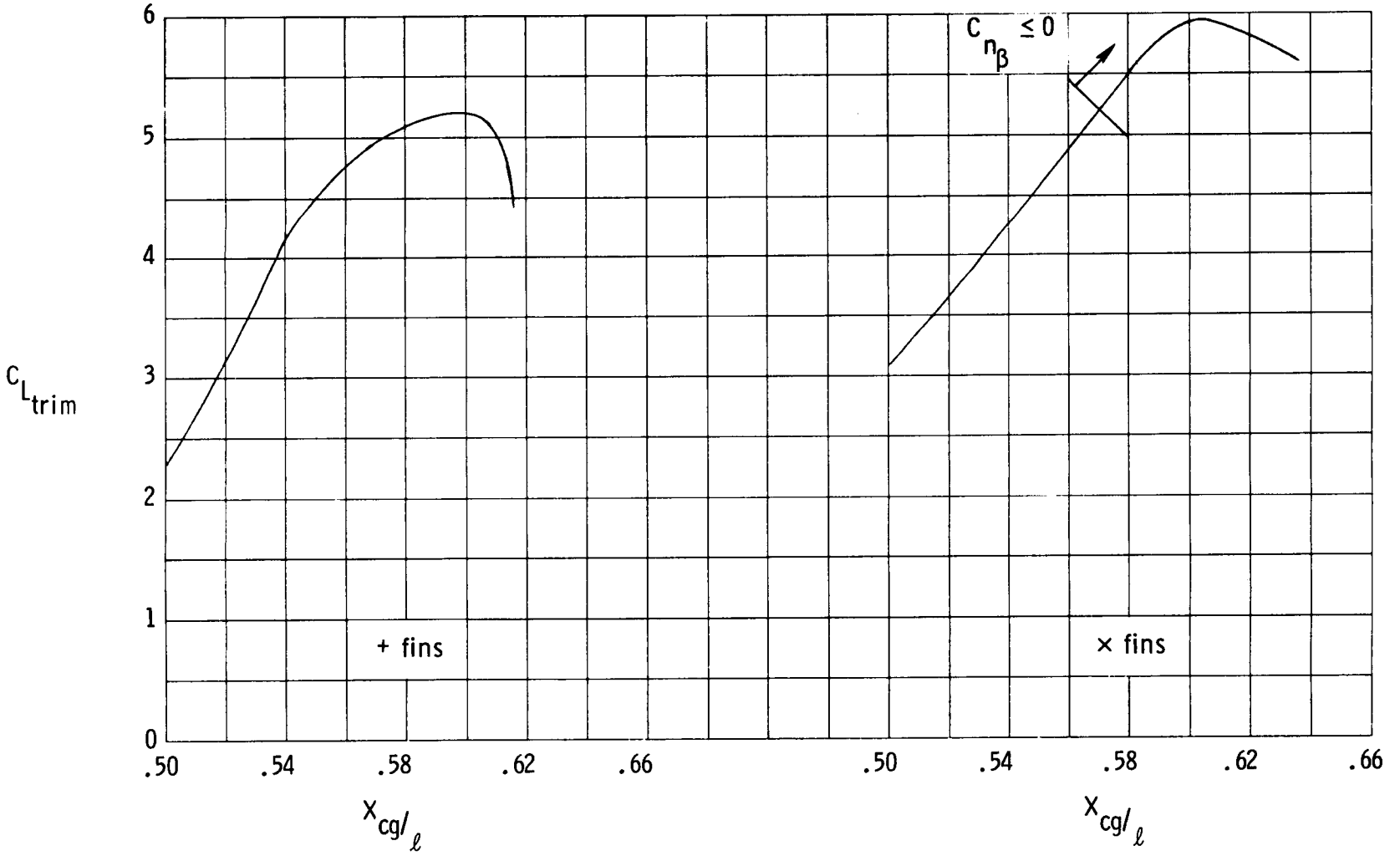

Figure 14. - Effect of center-of-gravity location on attainable lift coefficient.

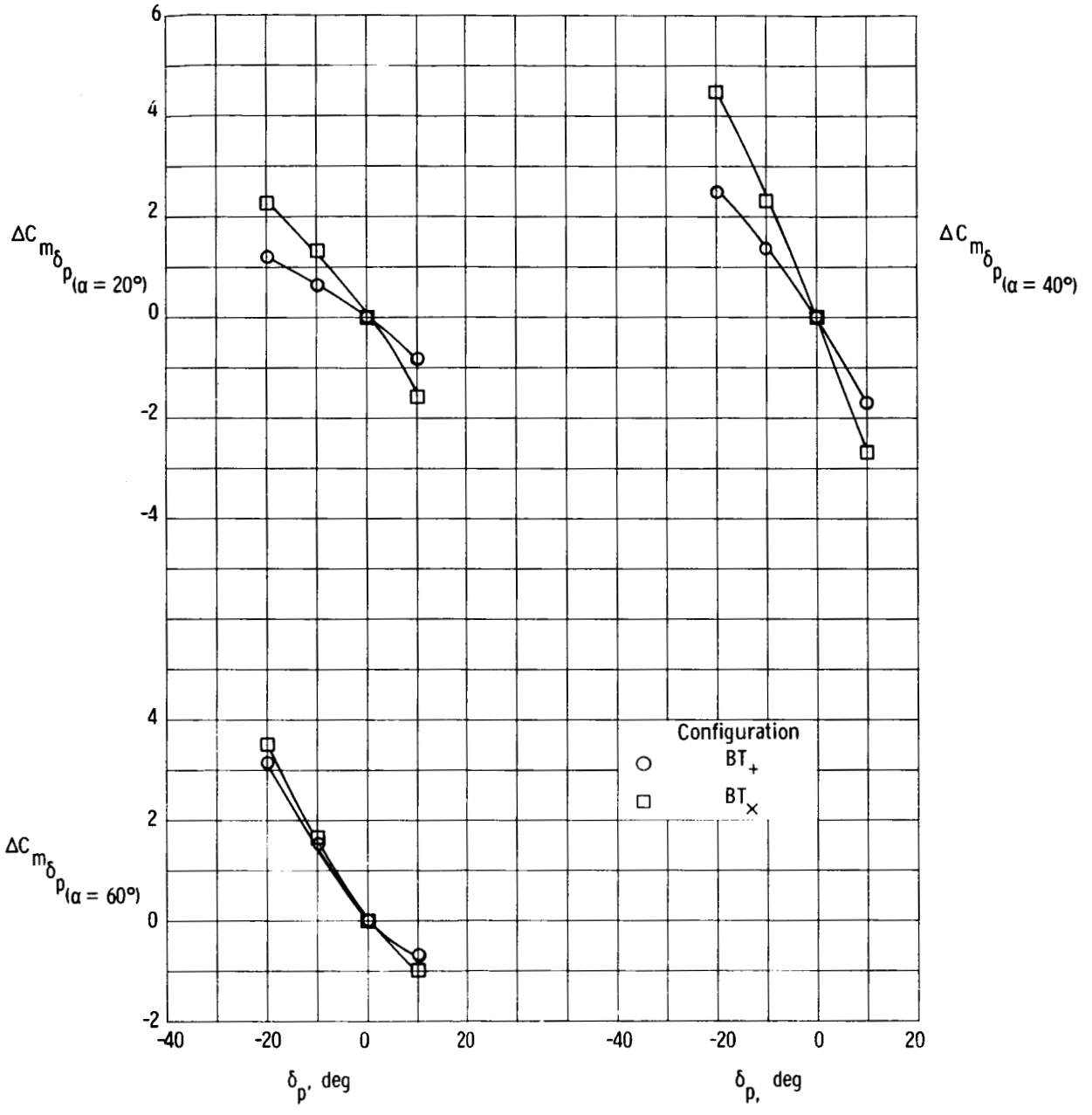

Figure 15. - Control power of fins for various angles of attack.

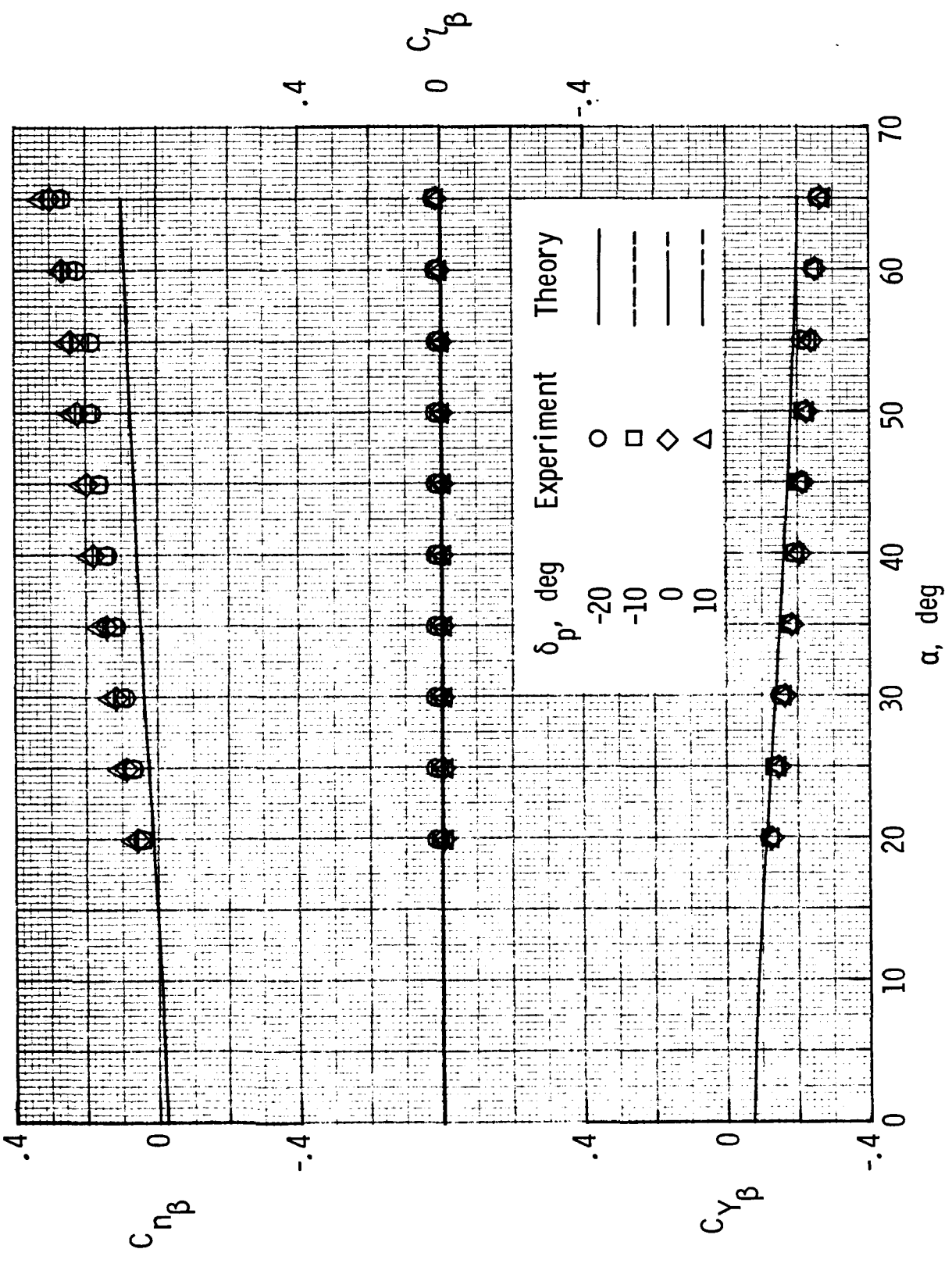

(a) + fins.

Figure 16. - Effect of pitch-control deflection on sideslip derivatives.

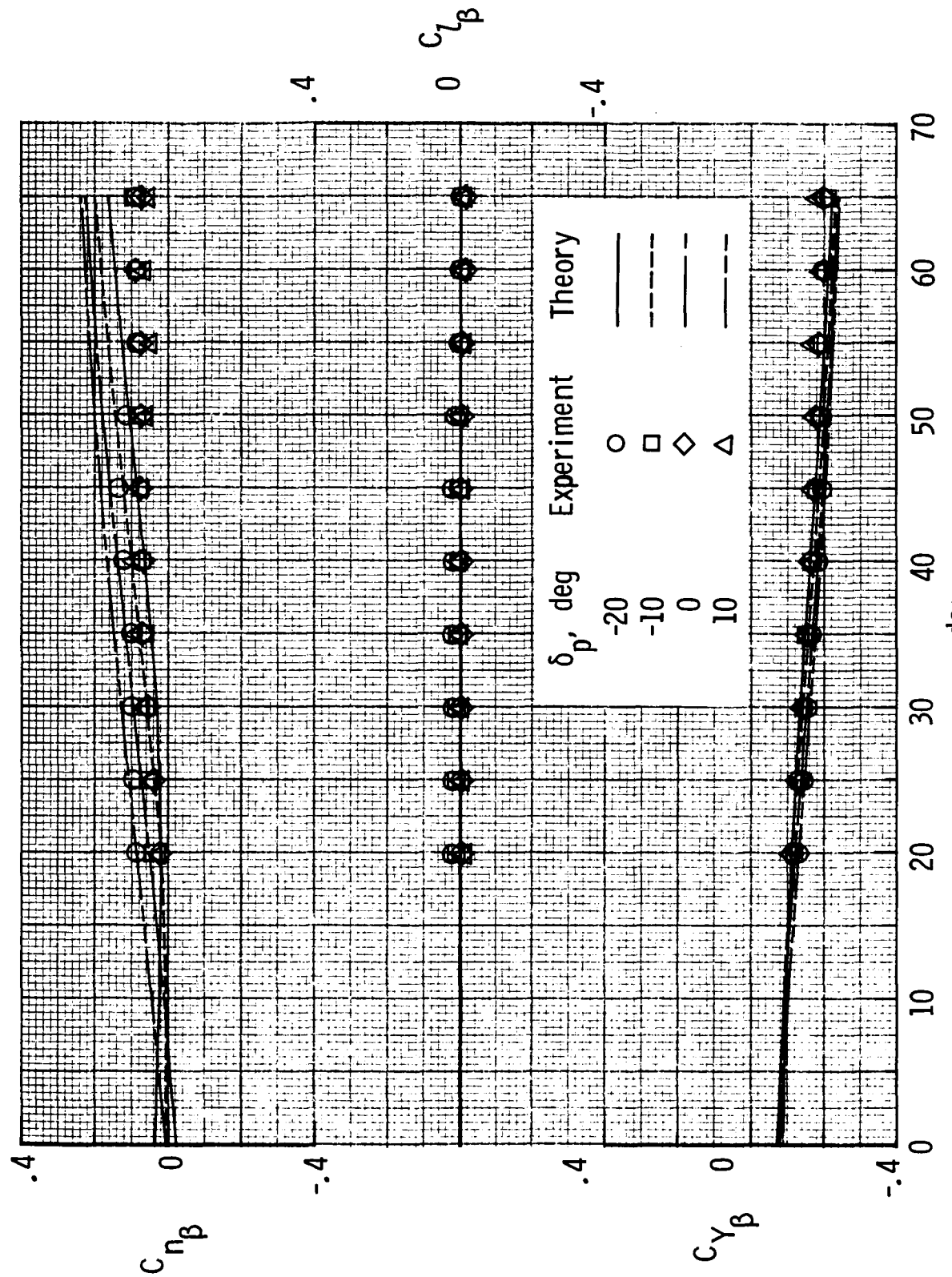

(b) x fins.

Figure 16. - Concluded.

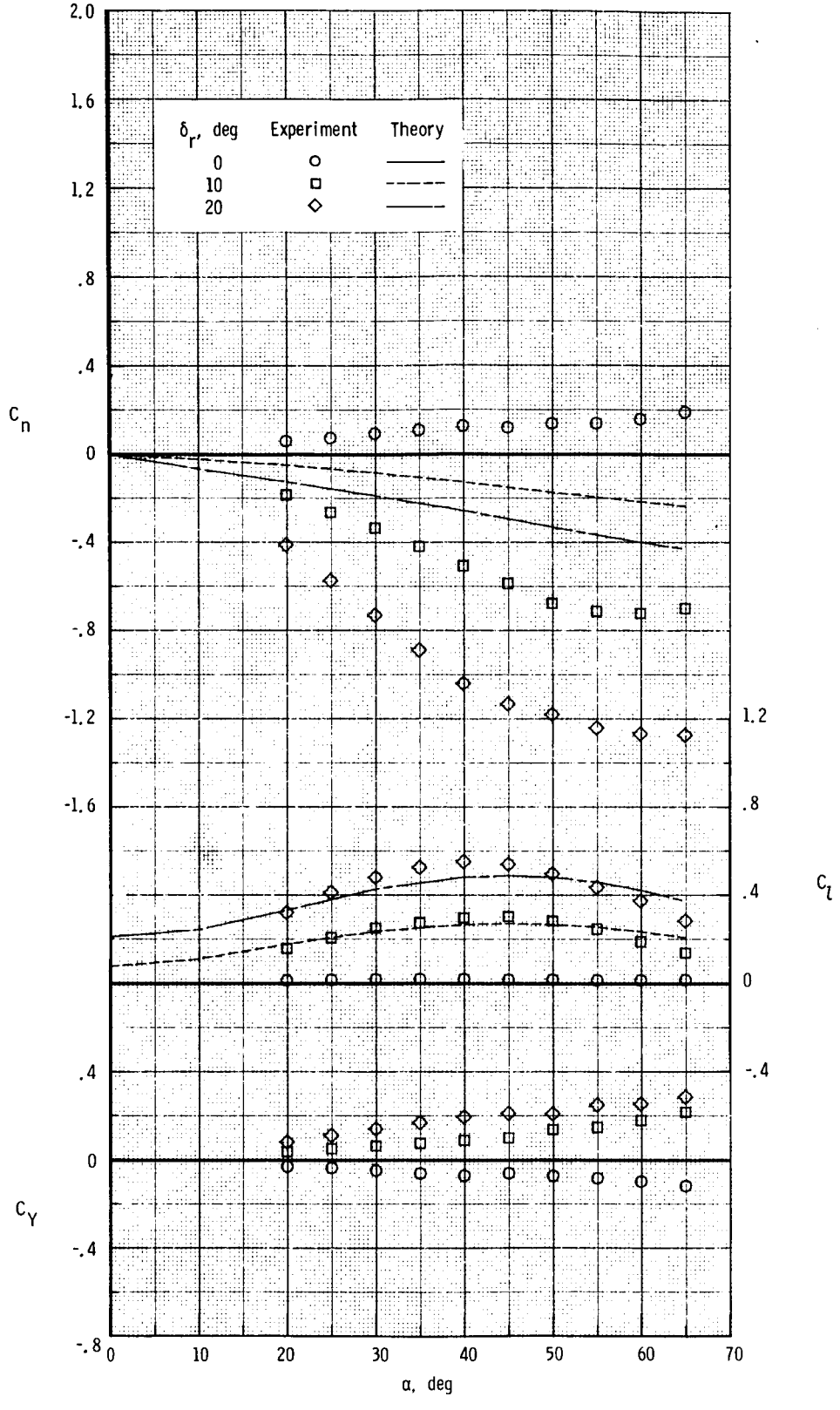

(a) + fins.

Figure 17. - Roll-control characteristics.

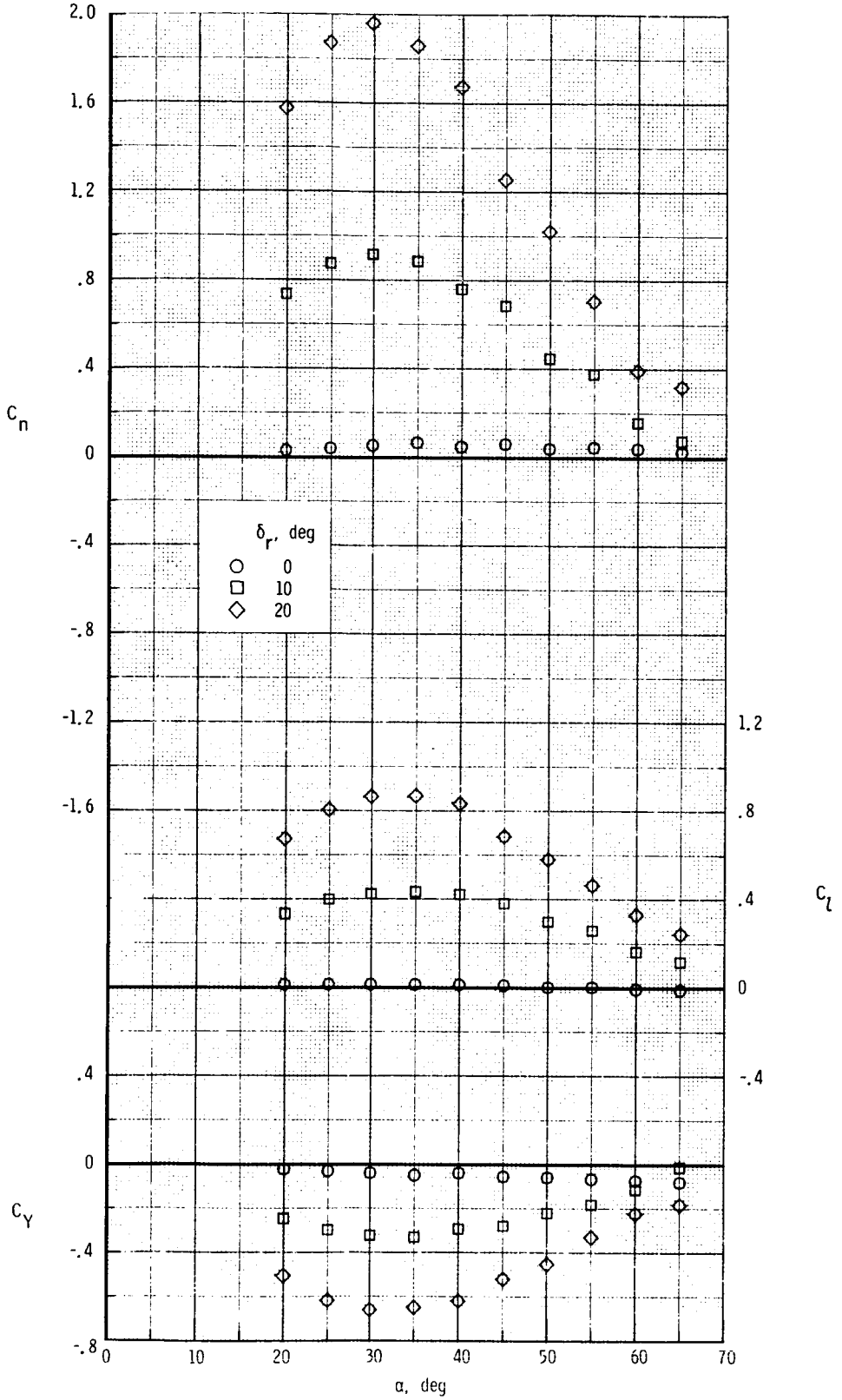

(b) ✕ fins.

Figure 17. - Concluded.

Standard Bibliographic Page

1. Report No.	2. Government Accession No.	3. Recipient's Catalog No.
NASA TM-89050		

4. Title and Subtitle	5. Report Date
Mach 6 Experimental and Theoretical Stability and Performance of a Finned Cylindrical Body at Angles of Attack Up to 65°	September 1986
	6. Performing Organization Code: 505-62-81-07
7. Author(s): Edward R. Hartman and Patrick J. Johnston	8. Performing Organization Report No.
9. Performing Organization Name and Address: NASA Langley Research Center, Hampton, VA 23665-5225	10. Work Unit No.
	11. Contract or Grant No.
12. Sponsoring Agency Name and Address: National Aeronautics and Space Administration, Washington, DC 20546	13. Type of Report and Period Covered: Technical Memorandum
	14. Sponsoring Agency Code

15. Supplementary Notes

16. Abstract

A theoretical and experimental investigation of the longitudinal and lateral-directional stability and control of a finned cylindrical body has been conducted at Mach 6. The angle-of-attack range extended from 20° to 65° to encompass maximum lift. Stability, performance, and trim could be accurately predicted with the fins in the + arrangement but this was not the case when the fins were in the × orientation where windward fin choking occurred at angles of attack above 50° reducing their effectiveness and causing pitch up.

17. Key Words (Suggested by Authors(s))	18. Distribution Statement
Hypersonic Finned body Stability and performance Large angles of attack	Unclassified - Unlimited Subject Category 02

19. Security Classif.(of this report)	20. Security Classif.(of this page)	21. No. of Pages	22. Price
Unclassified	Unclassified	44	A03

For sale by the National Technical Information Service, Springfield, Virginia 22161